Ceramics International 49 (2023) 11005–11017

Contents lists available at ScienceDirect

Ceramics International

journal homepage: www.elsevier.com/locate/ceramint

Multiphase zinc and magnesium mono-substituted calcium phosphates derived from cuttlefish bone: A multifunctional biomaterials

Antonia Ressler [a,b,*], Tomislav Ivanković [c], Irena Ivanišević [a], Matija Cvetnić [a], Maja Antunović [a], Inga Urlić [c], Hrvoje Ivanković [a], Marica Ivanković [a]

[a] Faculty of Chemical Engineering and Technology, University of Zagreb, HR-10001, Zagreb, Marulićev trg 19, p.p.177, Croatia
[b] Faculty of Engineering and Natural Sciences, Tampere University, Korkeakoulunkatu 6, P. O. Box 589, 33014, Tampere, Finland
[c] Faculty of Science, University of Zagreb, HR-10000, Zagreb, Horvatovac 102a, Croatia

ARTICLE INFO

Keywords:
Antibacterial activity
Biomimetic
E. coli
Hydroxyapatite
Magnesium
Octacalcium phosphate
S. aureus
Zinc

ABSTRACT

Biomimetic calcium phosphate (CaP) systems mono-substituted with zinc (Zn^{2+}) and magnesium (Mg^{2+}) ions were prepared from a biogenic source (cuttlefish bone) by wet precipitation method. The results revealed that the as-prepared powders were composed of calcium-deficient carbonated hydroxyapatite (HAp), octacalcium phosphate (OCP), and amorphous calcium phosphate (ACP), while the heat-treated powders consisted of HAp, α-tricalcium phosphate (α-TCP), and β-tricalcium phosphate (β-TCP). In addition to Zn^{2+} and Mg^{2+} ions, the presence of CO_3^{2-}, Sr^{2+} and Na^{+} ions was detected with elemental analysis, which can be attributed to the use of cuttlefish bone as a natural precursor of Ca^{2+} ions. The data obtained by XRD study demonstrated the decrease in lattice parameters in the OCP and β-TCP phases for Zn-substitution and Mg-substitution in the HAp, OCP, and β-TCP phases. Zn^{2+} occupies the Ca(1,3,4,6,7,8) sites in OCP and Ca(1,2,3,4) sites in β-TCP, while Mg^{2+} occupies the Ca(2) sites in HAp and the Ca(4,5) sites in β-TCP. Phase transformation study under simulated physiological conditions for 7 days showed the transformation of OCP and ACP into the thermodynamically more stable HAp. Characterization of the zeta-potential showed positively charged populations for all prepared CaP powders, while all samples showed high bovine serum albumin adsorption capacity. The culture of human embryonic kidney cells showed that the prepared CaPs are non-cytotoxic and that viability of the cells increases during the culture period. All powders obtained showed antibacterial activity towards Gram-negative *Escherichia coli* and low antibacterial effect against Gram-positive *Staphylococcus aureus*, as determined by viability analysis during 48 h. Inhibition zone analysis and observation of the morphology after 24 h showed no antibacterial properties.

1. Introduction

Calcium phosphate (CaP) ceramics are used as bone grafting materials because they promote rapid bone formation and healing of bone defects. Calcium and phosphate ions have a direct influence on bone cells and can induce cell attachment, proliferation, and differentiation [1]. The most commonly used CaP as a bone graft material is hydroxyapatite ($Ca_{10}(PO_4)_6(OH)_2$, HAp) because its chemical structure is the most similar to the natural bone mineral. HAp can bond directly to the bone and has good biocompatibility and bioactivity [2]. Numerous studies are still focused on finding a suitable approach to improve the biological properties of CaPs [3,4]. Biphasic, triphasic, and multiphasic CaP systems, in which the bone graft usually contains HAp, octacalcium phosphate (OCP), amorphous calcium phosphate (ACP), α-tricalcium phosphates (α-TCP), and β-tricalcium phosphates (β-TCP), are receiving increasing attention. There are no major differences in the mechanical, physical, and chemical properties of biphasic, triphasic, or multiphasic CaP systems; however, the major difference is related to the *in vivo* bioresorption behaviour as the biodegradation rate can be altered by adjusting the weight ratio of the phase composition [5,6].

In addition to multiphase CaP systems, ionic substitutions in CaP can result in a chemical composition similar to biological apatite, which can further improve the biological properties. Naturally occurring apatite contains various amounts of trace elements such as sodium (Na^{+}, 1.0 *wt*

* Corresponding author. Faculty of Engineering and Natural Sciences, Tampere University of Technology, P. O. Box 589, 33101, Tampere, Finland.
E-mail addresses: aressler@fkit.hr, antonia.ressler@tuni.fi (A. Ressler), tomislav.ivankovic@biol.pmf.hr (T. Ivanković), ivanisevic@fkit.hr (I. Ivanišević), mcvetnic@fkit.hr (M. Cvetnić), maja.antunovic2007@gmail.com (M. Antunović), inga.urlic@biol.pmf.hr (I. Urlić), hivan@fkit.hr (H. Ivanković), mivank@fkit.hr (M. Ivanković).

https://doi.org/10.1016/j.ceramint.2022.11.295
Received 14 September 2022; Received in revised form 17 November 2022; Accepted 23 November 2022
Available online 28 November 2022
0272-8842/© 2022 The Authors. Published by Elsevier Ltd. This is an open access article under the CC BY license (http://creativecommons.org/licenses/by/4.0/).

%), potassium (K^+, 0.07 *wt*%), magnesium (Mg^{2+}, 0.6 *wt*%), strontium (Sr^{2+}, 0.05 *wt*%), zinc (Zn^{2+}, 39 ppm), silicon (SiO_4^{4-}, 500 ppm) and carbonate (CO_3^{2-}, 4.8 *wt*%) ions [7]. Zinc is crucial for the synthesis of alkaline phosphatase (ALP), which is released by osteoblastic cells in the early phase of bone maturation and for creating an alkaline environment that promotes the precipitation of inorganic phosphates [3]. Zn-substituted CaP decreases the osteoclast resorption process, increases osteoblast activity, promotes the bone formation process, and possesses anti-microbial and anti-inflammatory properties [8–10]. Magnesium is especially important in the early phase of bone formation, where it acts as a growth factor and is crucial for enzyme production, while magnesium deficiency leads to cessation of bone growth, bone fragility, and osteoporosis, decreasing osteoblast activity and increases osteoclast activity. Magnesium is quantitatively one of the most important metal ions in bone tissue, and its concentration decreases with increasing calcification [9,11–13].

Even though CaPs as biomaterials have shown the desired properties for bone regeneration, the development of biofilms on the surface of the biomaterials often leads to infections that require medical intervention and may result in revision surgery. The current approach to address this concern is through the usage of antibiotics, but they do not act at the specific site of infection. A better approach is to use biomaterials that prevent biofilm formation in order to avoid need for antibiotics [14]. Due to its antibacterial properties, zinc is considered as a promising substitution element in the CaP lattice to control bacterial adhesion and biofilm formation [14,15]. The use of substituents with antibacterial properties (e.g., Zn^{2+}, Ag^+, Cu^{2+}), can avoid the usage of antibiotics. This is extremely important nowadays since the overuse of antibiotics, has led to the rapid spread of antibiotic resistance [16,17].

Considering the importance of zinc and magnesium for bone development, the aim of this study is the synthesis and characterization of zinc and magnesium substituted multiphase CaP systems by following a biomimetic approach. CaPs obtained from biogenic sources are better accepted by human organism because of its physiochemical similarity to biological apatite [18]. Natural resources comprised of calcium carbonate ($CaCO_3$) such as corals, seashells, eggshells and cuttlefish bone are receiving growing interest as they can be converted to CaP. Biogenic sources are low-cost materials available worldwide and by using waste materials circular economy approach is followed [18–20]. In the present study, biogenic $CaCO_3$ (calcite), obtained from cuttlefish bone, was used as a source of Ca^{2+} ions to obtain CaPs that mimic the physio-chemical properties of the natural bone mineral. In our previous studies [21,22], CaP systems substituted with Sr^{2+} and SeO_3^{2-} ions have been prepared from cuttlefish bone, a bio-waste, which is why this low-cost synthesis is considered an environmentally friendly approach [23]. The effects of Zn^{2+} and Mg^{2+} substitution on the phase content, crystal shape, elemental distribution, lattice parameters, Ca sites occupancy, thermal stability, zeta potential, protein adsorption and cell proliferation have been investigated. To determine the bioactivity, phase transformation was monitored after 7 days of incubation in simulated body fluid at 37 °C. In addition, antibacterial activity against Gram-positive *Staphylococcus aureus* (*S. aureus*) and Gram-negative *Escherichia coli* (*E. coli*), representative bacteria in clinical bone infections, has been evaluated.

2. Materials and methods

2.1. Synthesis of substituted calcium phosphates

Non-substituted, Zn-substituted and Mg-substituted CaP powders were prepared by wet precipitation method under mild conditions. $CaCO_3$ obtained from cuttlefish bone was used as a precursor of Ca^{2+} ions, prepared as described in our previous papers [21,22]. In addition, an appropriate amount of zinc nitrate hexahydrate ($Zn(NO_3)_2 \cdot 6H_2O$; Honeywel) or magnesium chloride hexahydrate ($MgCl_2 \cdot 6H_2O$, KEMIG) and $CaCO_3$ were dissolved/resuspended in acetic acid aqueous solution (pH = 4.60, 40 °C). The selected molar ratios of Zn/(Ca + Zn) and Mg/(Ca + Mg) were 0, 0.01, and 0.05, and the samples were designated as CaP_0, CaP_Zn1, CaP_Zn5, and CaP_0, CaP_Mg1, CaP_Mg5, respectively. The numbers in sample labels (0,1 and 5) are the nominal Zn or Mg mol.% values expected to be substituted into hydroxyapatite (in place of Ca). According to the literature [24–26] and preliminary studies, in the selected range of M/(Ca + M) molar ratios, no secondary phases characteristic for zinc and magnesium (other than CaPs) were expected.

Ammonium dihydrogen phosphate ($NH_4H_2PO_4$; Lachner) was added into the solution to gain a molar ratio (Ca + Zn)/P and (Ca + Mg)/P of 1.67 (stoichiometric HAp). Stirring was continued at 60 °C for 3 days, followed by overnight aging at room temperature (T = 24.0 ± 0.3 °C). The as-prepared CaP particles were separated from supernatant by filtration without washing. Part of each sample was heat-treated at 1200 °C for 2 h.

2.2. Powder characterization

The final pH of non-substituted, Zn-substituted and Mg-substituted CaP suspensions was measured on Schott CG 842 pH-meter using BlueLine 14 electrode with the precision of 0.01 at room temperature (T = 24 ± 0.3 °C).

Fourier transform infrared spectra (FTIR) of as-prepared powders was recorded by attenuated total reflectance (ATR) spectrometer for solids with diamond crystal (Bruker Vertex 70) at 20.0 °C, over the spectral range of 4000-400 cm^{-1}, with 32 scans and a resolution of 4 cm^{-1}.

The powder morphology for all as-prepared powders was analyzed by scanning electron microscopy (SEM, TESCAN VEGA3 Easyprobe) at an electron beam energy of 13 keV. EDS analysis was performed at an electron beam energy of 20 kV, to investigate the elemental composition of the surface of the CaP_Zn5 and CaP_Mg5 powders. Prior to analysis, dried crystals were coated with a gold and palladium plasma for 60 s.

Elemental analysis was performed by inductively coupled plasma mass spectrometry (ICP-MS, PerkinElmer SCIEXT ELANR DRC-e, Concord, Canada) according to the manufacturer's protocol. The accuracy of ICP-MS was verified with standard reference materials (ICP-MS Complete Standard-V-ICPMS-71A, Inorganic Ventures, USA) and the results for all relevant elements were within the certified concentration range. 100 mg of each sample was dissolved in 1 ml of aqueous HNO_3 solution (Ultra-Pure, Sigma Aldrich) and the solution volume was increased to 10 ml with ultrapure water. The carbon content in the as-prepared powders was determined with a total organic carbon analyzer (TOC) using the Shimadzu TOC V-Series. Samples were dissolved in an aqueous H_2SO_4 solution (Sigma Aldrich), from which dissolved CO_2 had previously been removed.

The as-prepared and heat-treated powders were mixed with 5 wt% polycrystalline silicon standard (NIST SRN 640e, Sigma Aldrich) and phase analysis was performed on a Shimadzu XRD-6000 diffractometer with Cu K_α (1.5406 Å) radiation operated at 40 kV and 30 mA. The analysis was performed in the range of diffraction angels between 3° and 60° for as-prepared samples, and between 20° and 70° for the heat-treated samples, with a 2Θ step of 0.02° and an exposure time of 10s.

2.3. Rietveld refinement studies

The software DIFFRAC.SUITE TOPAS V.5.0. with the fundamental parameter approach was employed for Rietveld refinements, as described in our previous work [21,22]. The structural parameters of hydroxyapatite determined by Veselinović et al. [27], octacalcium phosphate by Espanol et al. [28], β-tricalcium phosphate by Yashima et al. [29] and α-tricalcium phosphate by Mathew et al. [30] were used as initial values for the refinements. The refined parameters were the scale factor, specimen displacement, bond length, mean crystallite size (Lvol-IB; the volume averaged column height), lattice parameters and occupancy factors. The P, O and H sites were kept fixed for all

refinements, resulting in improved refinement of Ca sites occupancy. The weighted profile (R_{wp}) and expected (R_{exp}) R-factor were used to assess the goodness-of-fit of the Rietveld refinement. The results with $R_{wp} < 10\%$ and $R_{exp} < 3\%$ were considered acceptable.

2.4. Protein adsorption assay of substituted CaP powders against BSA

Protein adsorption of bovine serum albumin (BSA, Sigma Aldrich, ≥96%) to the prepared CaP powders was performed according to the protocol described by Shi et al. [31]. In brief, 10 mg of the synthesized CaP powders ($n = 3$) were dispersed in 1 ml of 250 μg/ml protein solution and incubated at 37°C for 4 h. After incubation, 25 μl protein supernatant was transferred to a 96-well cell culture plate containing a 200 μl BCA working agent. The plate was mixed on a plate shaker for 30 s and kept at 37 °C for 30 min. Analysis was performed using a micro-plate reader (GlowMax-Multi, Promega) at 560 nm. Results were expressed as a percentage (%) of adsorbed protein relative to control (250 μg/ml, protein/PBS).

2.5. Zeta-potential measurement

Zeta-potential (Zetasizer Ultra, Malvern Pananalytical, UK) of the obtained pure CaP, Zn- and Mg-substituted CaP particles were determined in phosphate buffer solutions (PBS) with different pH values. Powdered products were suspended in PBS and dispersed using a Sonopuls HD3200 (Bandelin, Germany) ultrasonic homogenizer and a MS 73 sonotrode. Suspension concentration was 0.1 mg/mL. Measurements were performed in a thermostated sample cell (DTS1070) with a total of 11 runs per sample, and the average values were reported. Prior to measurement, all CaP samples were equilibrated at 25.0 ± 0.1 °C for 60 s. ZS Xplorer software was used for method set-up and data evaluation.

2.6. Phase transformation

As-prepared CaP_0, CaP_Zn5 and CaP_Mg5 powders were incubated in static simulated body fluid (SBF) to determine phase transformation at 37 °C. The SBF solution was prepared as previously described by Bohner and Lemaitre [32]. 100 mg of each powdered samples were immersed in 10 ml of SBF at 37 °C for 7 days. After incubation, the samples were washed in demineralized water and dried at room temperature (T = 24.0 ± 0.3 °C). Phase analysis of the powders after incubation was determined by XRD analysis and Rietveld refinement studies.

2.7. Biological evaluation

2.7.1. Preparation of extracts of CaP powders

The human embryonic kidney 293 cells (HEK 293, Sigma Aldrich) were used to determine the biocompatibility of as-prepared powders (CaP_0, CaP_1 Mg, CaP_5 Mg, CaP_1Zn, and CaP_5Zn). CaP powders were sterilized for 15 min under UV light and incubated for 24 h at 4 °C with Dulbecco's modified Eagle's culture medium (DMEM) – high glucose (Sigma-Aldrich) supplemented with 10% fetal bovine serum (Capricorn Scientific) and 1% penicillin/streptomycin (Lonza) at a concentration of 10 mg/mL. After incubation, the powders were centrifuged (300×*g*) for 5 min in order to spin them down, while the supernatant was used for cell feeding.

2.7.2. Cell culture

HEK 293 cells were thawed from liquid nitrogen and seeded into a 75 cm^3 flask in the medium until confluence. After reaching confluence, cells were trypsinized with Tripsin/EDTA (Sigma-Aldrich) to obtain a cell suspension. The concentration of 5×10^5 cells/200 μl of the medium was seeded in each well (96-well plate, Sarsted) and incubated for 24 h in humidified atmosphere of 5% CO_2 at 37 °C. The following day, the medium from each well was replaced with the supernatant of CaP powders and kept under cell culture conditions for 1 and 3 days in. The medium from the control cells was replaced with fresh cell culture medium, respectively.

2.7.3. Cytotoxicity evaluation by MTT assay

Viability of HEK-293 cells was determined using the MTT (3-(4,5-dimethylthiazol-2-yl)-2,5-diphenyltetrazolium bromide) assay (Sigma-Aldrich), after 1 and 3 days of the incubation. After the designated time points, the medium/extracts were removed and 40 μl of MTT solution was added to each well. After 3 h at 37 °C, 170 μl of dimethyl sulfoxide (DMSO, Sigma-Aldrich) was added to each well. Once the formazan crystals had dissolved, the solution was set for colorimetric detection at 560 nm using a microplate reader (GlowMax-Multi, Promega). All experiments were performed in triplicates. The percentage of cell viability was calculated from the absorbance values in reference to the untreated cells (control).

2.7.4. Quantitative detection of live cells (%) by live dead cell assay

After the designated time points, the culture medium/extracts were removed while the cells from each well were collected by trypsinization and placed in Eppendorf tubes. Cells were washed with PBS (Gibco) and then incubated with 200 μl of × 1000 diluted *live/dead* assay staining solution (Abcam). After 10 min of incubation in the dark, the cell suspension from each tube was transferred into each well. The black opaque 96-well plates (Corning) were used. The green fluorescence of the live cells was detected on a microplate reader (GlowMax-Multi, Promega) using a fluorescence filter (excitation 490 nm, emission 510-570 nm). All experiments were performed in triplicates. The percentage of live cells was calculated from the fluorescence readings in reference to the untreated cells.

2.8. Antibacterial activity

The antibacterial efficacy of the tested material was determined by widely used agar diffusion also known as the Kirby-Bauer test, and the viable cell assay. As the model organisms, the bacteria *Staphylococcus aureus* (*S. aureus*), strain ATCC 25923, and the *Escherichia coli* (*E. coli*), strain DSM 498, were used. Prior to each experiment, the pure cultures of bacteria were revitalized by growing them for 24 h at 37°C on LB agar plates (the composition was tryptone 10 g, yeast extract 5 g, NaCl 5 g, agar 15 g, 1 L of deionized water). Otherwise, the bacteria were kept as axenic cultures in a cryo-storage system, the Microbank® (Pro-Lab Diagnostics, Round Rock, USA).

2.8.1. Agar disc diffusion assay

This test was performed according to the standardized methodology for antibiotic testing (EUCAST). First, bacterial suspensions of ~3×10^8 cells per ml (0.5 McFarland) in sterile saline (0.9% NaCl) were prepared. Next, bacteria were smeared all over the LB agar plate as to grow the so-called bacterial lawn. This was done by using a sterile swab stick. Next, and prior to incubation, the material samples were placed onto the agar surface. The samples were in the form of 14 mm diameter discs, made by cold pressing (250 MPa) of CaP powders. After the incubation for 24 h at 37°C, the agar plates were checked for clear zones of no growth around the discs. If the sample is releasing an antibacterial compound, it either kills or stops the bacteria growing in a circular zone around the sample. The zone is larger if the antibacterial compound is more effective. The zones around all the samples were measured and samples were compared for their antibacterial efficacy.

2.8.2. Surface morphology after diffusion assay

In order to examine what happened with bacteria during 24 of contact with the samples, the discs from the agar-diffusion assay after the incubation were subjected to SEM analysis of surface morphology at TESCAN Vega3 EasyProbe at electron beam energy of 7 keV. The discs

Table 1
Results of ICP-MS and TOC analysis.

	Minor substituents (*mol*%)					Ca + M/P (*mol/mol*)		M/Ca + M (*mol/mol*)	
	Zn	CO_3^{2-}	Na	Mg	Sr	solution	powder	solution	powder
CaP_0	0.00	8.16	3.66	0.28	0.48	1.60	1.69	0.003	0.003
CaP _Zn1	1.12	7.20	3.47	0.54	0.46	1.60	1.70	0.012	0.011
CaP _Zn5	5.90	3.86	4.54	1.10	0.57	1.57	1.40	0.063	0.059
CaP _Mg1	0.00	5.06	4.33	1.52	0.56	1.59	1.59	0.016	0.015
CaP _Mg5	0.00	3.82	3.82	5.16	0.57	1.60	1.60	0.054	0.052

were prepared for the scanning by dehydration, as follows: the round samples were carefully lifted off the agar surface and aseptically placed into a sterile 30 mm Petri dish so that the side in contact with the inoculated agar was facing up. Next, fixation of cells was done by pouring paraformaldehyde (Sigma Aldrich) solution (2%) in PBS (Sigma Aldrich) into the Petri dish and allowed to settle for 24 h at 4 °C. The samples were then washed with sterile PBS and dehydrated in a series of ethanol (Sigma Aldrich) solutions as follows; 30%/2 min, 50%/2 min, 70%/5 min, 96%/5 min, 99.9%/5 min, 99.9%/5 min. Finally, dehydrated samples were dried at 50 °C for 30 min. For presentation, the bacteria and sample substrate were false-colored in Adobe Photoshop CC 2018.

2.8.3. Viable cell assay

Final step was to determine the antibacterial efficacy of the material samples by the viable cell assay. A bacterial suspension of ~10^6 bacterial cells per ml of *S. aureus* or *E. coli* in 0.9% NaCl saline was distributed to a series of plastic vials. To each vial, a 0.25 g of the powdered sample was added and vials were incubated at room temperature on a rotating shaker (Stuart) at 4 rpm for 3 days. After 3, 6, 24, 48 and 72 h, an aliquot of 100 μl was taken from the vial, serially diluted, plated on LB agar and incubated at 37 °C for 24 h. The grown colonies were counted and the number of cells was expressed as CFU ml^{-1}. Finally, the amount of viable bacterial cells in the suspension after the specified contact time with the different powdered samples was compared.

2.9. Statistical analysis

Quantitative results are expressed as mean ± SEM (standard error of the mean). Statistical analysis was performed using a one-way ANOVA test considering the p-value <0.05 statistically significant.

3. Results and discussion

Biological calcium phosphate is non-stoichiometric calcium deficient HAp with foreign ions (Mg^{2+}, Zn^{2+}, Sr^{2+}, Na^+, HPO_4^{2-}, CO_3^{2-}) substituted in its structure. The physicochemical properties of synthetic biomaterials could be improved by mimicking the phases and chemical composition of biological minerals. Bioceramics partially or completely derived from biogenic sources (seashells, corals, cuttlefish bone, eggshells) are better accepted *in vivo* as they have similar properties to the natural bone apatite [17,33]. The advantages of using a biogenic source were indicated in the study by Kim et al. [34], where better biocompatibility *in vitro* and more defined bone regeneration *in vivo* of HAp synthesized from cuttlefish bone were observed, compared to commercial HAp. However, the physicochemical properties of used HAp powders were not analyzed, to give more insights into the chemical composition.

3.1. The chemical composition of as-prepared powders

The chemical composition of the as-prepared powders was determined by ICP-MS and TOC analysis. In Table 1, the mol% substitution of Ca^{2+} ions by Sr^{2+}, Mg^{2+}, Zn^{2+} and Na^+, and PO_4^{3-} by CO_3^{2-} ions in prepared CaPs was presented. Sr^{2+}, Mg^{2+}, Na^+ and CO_3^{2-} ions, which are typical substitution ions for bone mineral, were detected in all as-prepared powders obtained from cuttlefish bone. The ICP-MS analysis of the cuttlefish bone ($CaCO_3$) has shown that the concentration of Ca^{2+} ions in precursor was 277.91, Sr^{2+} ions 3.01, Mg^{2+} ions 0.67, Na^+ ions 51.12 and Zn^{2+} ions 0.01 mg/L. As a result of the presence of trace elements in cuttlefish bone, the ICP-MS analysis showed that the CaP_0 powder contains 0.48 mol% Sr^{2+}, 0.28 mol% Mg^{2+}, 3.66 mol% Na^+ and 8.16 mol% CO_3^{2-} ions, while Zn^{2+} ions were not detected. The substitution of Na^+ ions in the CaP lattice requires charge compensation defects to maintain the neutrality of the unit cell, while surrounding ions may undergo structural relaxation due to the ion radius difference [35]. Charge compensation can occur with simultaneous substitution of Na^+ at Ca^{2+} sites, while PO_4^{3-} ions are substituted with CO_3^{2-} and/or HPO_4^{2-} ions [36]. Therefore, the presence of the Na^+ ions within the CaP system can lead to compensatory substitutions that can affect CaP formation as discussed later.

Due to the presence of magnesium in the non-substituted CaP_0 system, the content in all samples is higher than the nominal content, which is 0, 1 and 5 mol% for CaP_0, CaP_Mg1 and CaP_Mg5, respectively. Although the non-substituted CaP_0 system does not contain Zn^{2+} ions, its content in the CaP_Zn1 and CaP_Zn5 powders is higher than the nominal one. Alternatively, it could simply mean that the $CaCO_3$ obtained from cuttlefish bone contains various trace elements (Na^+, Mg^{2+} and Sr^{2+}), which result in a lower Ca content in the calcite. This leads to a lower amount of Ca^{2+} ions added in the reaction solution and therefore higher experimental degree of substitution (*mol*%) of Zn^{2+} ions. The biogenic precursor of Ca^{2+} ions is considered as a source of foreign ions in the obtained CaP, and the content of calcium, magnesium and zinc in the initial solution was corrected and the "real" molar ratios in the solution were calculated and compared with the corresponding ratios of the as-prepared powders. Due to the presence of foreign ions in the biogenic precursor and consequently in the initial solution, the real (Ca + M)/P ratio in the starting reaction mixture is lower than the value of 1.67 required for precipitation of stoichiometric HAp. The Zn/(Ca + Zn) and Mg/(Ca + Mg) ratios of the as-prepared powders are close to those of the initial solution, suggesting quantitative incorporation of magnesium and zinc into the precipitated phase.

The content of CO_3^{2-} ions (Table 1) in prepared samples decreases along with the increase of Zn^{2+} and Mg^{2+} substitution degree. The weight percentage of CO_3^{2-} ions in natural bone tissue is in the range of 4–8 *wt*% and depends on bone maturation [37]. According to Landi et al. [37], the use of $CaCO_3$ based biogenic sources (cuttlefish bone, seashells, eggshells) increases CO_3-substitution in CaPs. In addition, substitution of Ca^{2+} by Na^+ ion (present in biogenic sources) stimulates the B-type substitution as a result of charge balance according to the $Ca_{10-y}Na_y[(PO_4)_{6-y}(CO_3)_y](OH)_2$ formula [38]. Together with the Mg^{2+}, Zn^{2+}, CO_3^{2-} and Na^+ ions, the constant molar ratio of Sr^{2+} is determined in all obtained CaP samples prepared from biogenic source, as the aragonite structure of cuttlefish bone is stabilized with Sr^{2+} ions [39,40]. It has been suggested that single substituted CaPs exhibited better *in vitro* and *in vivo* properties than non-substituted systems. However, single-substituted CaP bioceramics do not provide the multiple functions required for clinical applications. Therefore, it can be assumed that a multi-substituted CaP system can lead to a multi-functional biomaterial that exhibits the beneficial effects of the individual substituents, e.g.

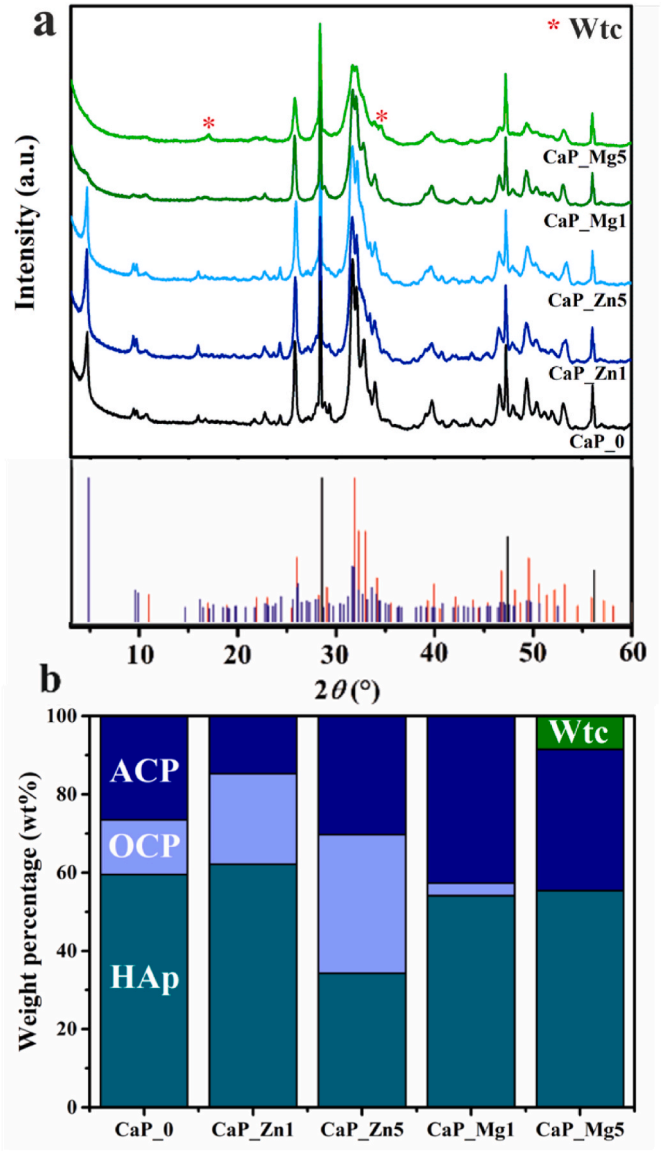

Fig. 1. XRD data of (a) the prepared CaP powders and (b) weight percentage of the precipitated phases obtained by Rietveld refinement analysis. The standard ICDD card data of hydroxyapatite (red), octacalcium phosphate (blue) and silicon (black, standard) are given below the XRD data. (For interpretation of the references to color in this figure legend, the reader is referred to the Web version of this article.)

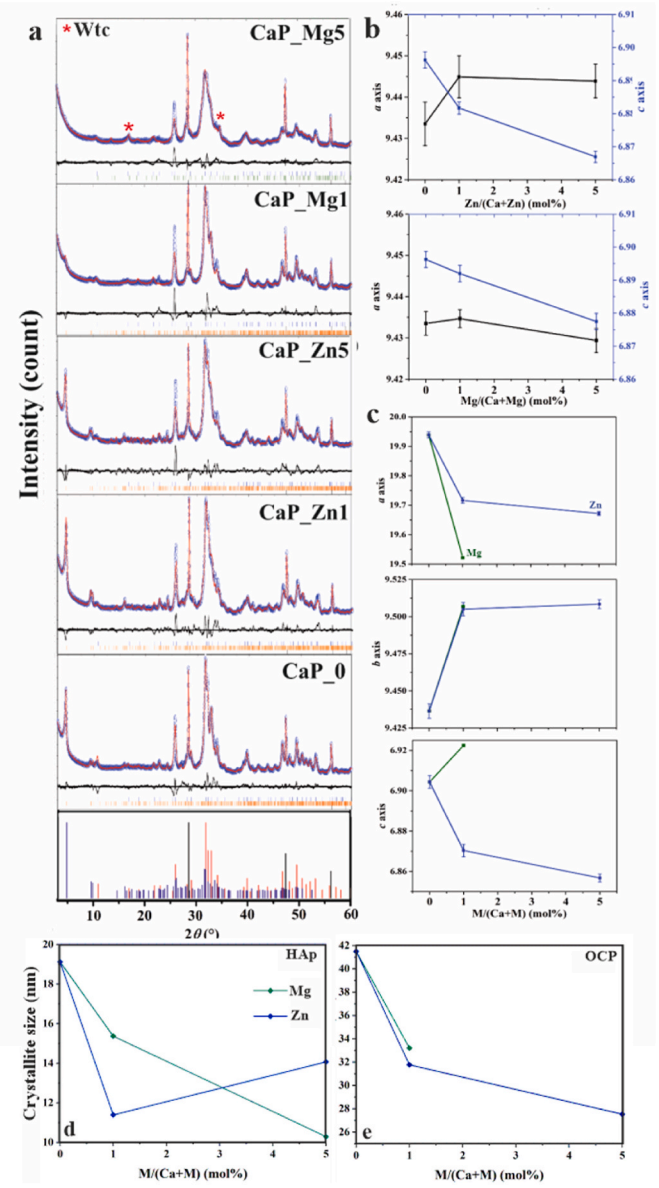

Fig. 2. (a) Rietveld analysis pattern of powder diffraction data for as-prepared Zn-substituted and Mg-substituted CaP powders. The open circles (blue) are experimental data and the solid lines (red) are calculated intensities. The difference between the experimental and calculated intensities is plotted below the profile. (b) Unit-cell parameters of HAp and (c) OCP phases obtained by Rietveld refinement of XRD data. The standard ICDD card data of hydroxyapatite (red), octacalcium phosphate (blue) and silicon (black, standard) are given below the XRD data. The crystallite size of HAp (d) and OCP (e) substituted with Zn^{2+} and Mg^{2+} ions determined by Rietveld refinement study. (For interpretation of the references to color in this figure legend, the reader is referred to the Web version of this article.)

enhancement of osteogenesis, antibacterial and anticancer efficacy [3]. Obtained results indicate that by using biogenic source (cuttlefish bone) multi-substituted CaPs is formed with similar element content as natural bone mineral.

3.2. XRD patterns of as-prepared powders and Rietveld refinements

The XRD patterns of as-prepared powders are shown in Fig. 1a. XRD peaks showed a good match to the line patterns for crystalline HAp (ICDD 09-0432) and OCP (ICDD 79-043). Polycrystalline silicon was used as an internal standard for qualitative phase analysis obtained by Rietveld refinement studies by using DIFFRAC.SUITE TOPAS V.5.0. software. The exception is the CaP_Mg5 powder in which instead of OCP phase the presence of Mg-substituted β-tricalcium phosphate ($Ca_9Mg(HPO_4)(PO_4)_6$) named whitlockite (Wtc, ICDD 70-2064) was detected, a phase that accounts for 25-35 wt% of the inorganic content of natural mineral tissue [41]. No additional peaks characteristic for zinc or magnesium compounds are observed for substituted CaP systems. The weight percentage (Fig. 1b) of HAp, OCP, Wtc, and amorphous calcium phosphate (ACP) phase, determined by Rietveld refinement analysis of the XRD patterns, is shown in Fig. 2a. The results indicate a significant amount of ACP in all prepared powders, ranging between 15 and 36%, as previously observed in our studies when the wet precipitation method was used [21,22].

ACP phase is a hydrated, thermodynamically unstable, transient phase that commonly precipitates during the formation of more stable CaPs in aqueous media. ACP is considered to be a precursor phase in

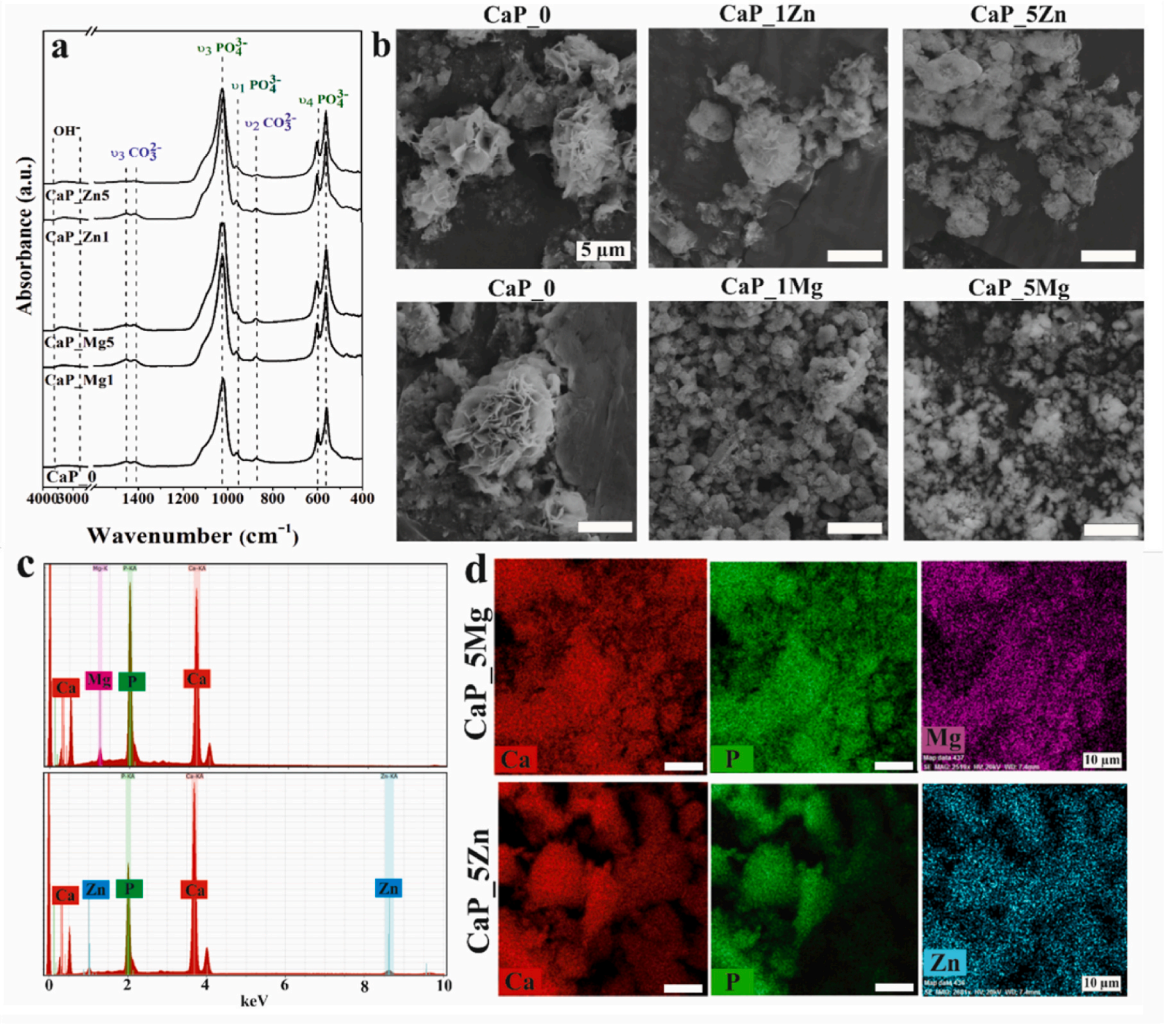

Fig. 3. (a) FTIR spectra of substituted CaP powders. (b) SEM micrographs of as-prepared CaP powders (scale bar: 5 µm). (c) EDX and (d) elemental mapping of the CaP_Zn5 and CaP_Mg5 samples (scale bar: 10 µm).

OCP formation. OCP is often found as an intermediate phase in the formation of thermodynamically more stable HAp. The final pH values of the prepared substituted suspensions between 8.7 and 9.2 favour precipitation of calcium-deficient HAp and ACP. OCP phase is more likely to be formed at the pH range 5.5–7 [42]. The presence of OCP phase in substituted CaPs at the pH value higher than 7.0 suggest that foreign ions influence the phase transformation of CaPs from amorphous to crystalline phases. Sugiura and Makita [43] investigated the role of Na^+ concentration in OCP formation from dicalcium phosphate dihydrate. With increasing Na^+ concentration in the solutions, the formation of OCP through hydrolysis was enhanced, while the formation of HAp was inhibited. Although not fully proven and confirmed, the generally accepted theory of the *in vivo* HAp formation mechanism is that ACP phase is first formed, which than converts to OCP phase and further hydrolyzes to a thermodynamically stable HAp phase [44,45]. In the literature, most of the studies are focused on the synthesis and properties of Mg^{2+} and Zn^{2+} substitutions in the single-phase system composed of HAp [17]. In this study, a multi-phase system of HAp, OCP and ACP was obtained, which resembles the phases found in natural bone mineral. HAp is still considered the most promising CaP for bone graft development. However, better biological properties of OCP *in vivo* compared to HAp were confirmed by many studies [44]. The *in vivo* studies by Suzuki et al. [46] suggested that the hydrolysis of OCP to apatite after implantation stimulates the differentiation of osteoblastic cells. The conversion occurs through the consumption of Ca^{2+} ions from the surrounding solution and the release of PO_4^{3-} ions in the solution. It is suggested that the co-expression of bone characteristic genes may be related to the PO_4^{3-} ions release during the conversion. Further *in vivo* studies by Suzuki's research group lead to the conclusion that biphase mixtures of OCP and ACP may further enhance osteogenic properties *in vivo* [47].

The lattice parameters of the HAp and OCP phases in the prepared powders, determined by Rietveld refinement of the XRD data, are shown in Fig. 2b and c, respectively. The lattice parameter *a* of the HAp phase in both Zn-substituted systems increased to similar value while the lattice parameter *c* decreased with increasing Zn content. Numerous studies have observed a decrease in cell parameters along with a simultaneous increase in the Zn dopant content as a result of substitution of Ca^{2+} ions. However, Friederichs et al. [8] observed a new position of the Zn^{2+} ion in the HAp lattice at the hexagonal axis 2*b* site, which led to an increase in the *c* axis and cell volume, while Miyaji et al. [48] explained the increase in cell parameters together with the Zn-dopand content by the substitution of OH^- groups by H_2O molecules.

The lattice parameters *a* and *c* of OCP decreased and the lattice parameter *b* increased with increasing Zn content. Decrease in the lattice parameters of the OCP phase might indicate that smaller Zn^{2+} (0.074 nm) ions have replaced Ca^{2+} (0.100 nm) ion at one of the crystallographic sites [9,49]. The lattice parameters $a = b$, and *c* of the HAp decrease with an increase of Mg^{2+} content. The lattice parameter *a* of the OCP phase in the CaP _Mg1 decreased, but *b* and *c* increased compared to

the CaP_0 values. According to Matsunaga [9] and Aina et al. [50] substitution with Mg^{2+} (0.072 nm) ions leads to a decrease in cell parameters due to the smaller ionic radius compared to Ca^{2+} ions. Obtained results are in agreement with the findings of Ren et al. [51] who reported that the maximum amount of Mg-substitution in the HAp structure is between 5 and 7 mol%, while, as reported by Suchanek et al. [52], a large amount of Mg^{2+} ions can stabilize the Wtc lattice. Further, Rietveld refinement allowed to conduct a quantitative identification of the HAp and OCP crystallite size in the obtained powders (Fig. 2d and e). In the prepared powders crystallite size for HAp is in the range of 10–20 nm, while for the OCP phase in the range of 28–42 nm. In both crystalline phases decrease of crystallite size is evident for substitution with Mg^{2+} and Zn^{2+} ions except for the 5 mol% Zn-substitution in HAp, where an increase in crystallite size was observed.

The difference in ionic radius of the substituted cations leads to distortion of the CaP lattice and consequently to a decrease in crystallinity and stability, and an increase in solubility [9,53]. As explained by Matsunaga [9], incorporation of Zn^{2+} and Mg^{2+} ions in HAp is limited, while the OCP structure is more resistant to impurities and can incorporate more foreign ions into its structure. The HAp structure exhibits a hexagonal structure and the $P6_3$ space group with two crystallographic sites for Ca atoms. The OCP structure is similar to those of HAp as it has almost the same positions of Ca atoms in the region of x = 0 – ¼ and x = ¾ – 1, which is why this region is called "apatite", between which the "hydrated" layer is located. The triclinic crystal structure of OCP, with the space group $P1$, has eight crystallographic Ca sites. The Ca3 and Ca4 sites are located in the hydrated layer of OCP, while the remaining Ca sites are located in the apatite layer [9].

Refinements indicated that Zn-substitution in the HAp structure did not occur at either Ca1 or Ca2 crystallographic site (data not shown). In the OCP phase, the Zn^{2+} ion occupied the Ca3, Ca4, Ca6, and Ca7 sites in CaP_Zn1, and the Ca4, Ca6, Ca7, and Ca8 sites in CaP_Zn5, respectively (Supplementary material, Table S1). The Mg^{2+} ion occupies the Ca2 site, and its occupancy increases along with the degree of Mg-substitution in the HAp phase (Supplementary material, Table S2). The occupation sites in the OCP structure could not be determined in CaP_Mg1 due to a small amount of precipitated OCP, while OCP was not detected at higher substitution levels. Previous theoretical and experimental studies by Matsunaga [9] and Bigi et al. [54] confirmed that smaller-sized ions (Zn^{2+} and Mg^{2+}) prefer the spatially smaller Ca2 site rather than the Ca1 site [9]. Our results are not in agreement with the findings of Ren et al. [55], who reported that Mg^{2+} is more difficult to incorporate into the apatite structure than Zn^{2+} ion.

Due to the lower coordination numbers and the smaller average bond length, the Ca5 and Ca6 sites are more favourable for the substitution of smaller-sized ions in the OCP structure. According to Matsunaga [9], ions of smaller size occupy Ca3, Ca5, Ca6 and Ca8 sites in the OCP structure. Thus, the main difference with the Matsunaga's study is the occupation of the Ca7 site. The results of the present study indicate that the Ca7 site has the shortest binding with oxygen and is therefore suitable for substitution. It could be hypothesised that the remaining portion of Zn^{2+} and Mg^{2+} ions, that are not substituted at the Ca crystallographic sites, are located in vacancies, adsorbed on the crystal surface, or remained in the ACP phase [9,56,57].

3.3. FTIR analysis

The FTIR spectra (Fig. 3a) of the as-prepared CaP powders show characteristic asymmetric stretching vibrations of P–O (ν_3) bands at 1018 cm^{-1}, asymmetric bending vibrations of O–P–O (ν_4) at 558 and 601 cm^{-1}, and symmetric stretching vibration of P–O (ν_1) at 964 cm^{-1}, which can be assigned to the PO_4^{3-} group of the HAp phase. In addition, the characteristic absorption band of an HPO_4^{2-} group at 1116 cm^{-1} can be assigned to the OCP or ACP phase in the prepared CaP systems [58–63]. The TOC analysis confirmed the presence of CO_3^{2-} groups in the prepared samples, which is manifested in the FTIR spectrum in the

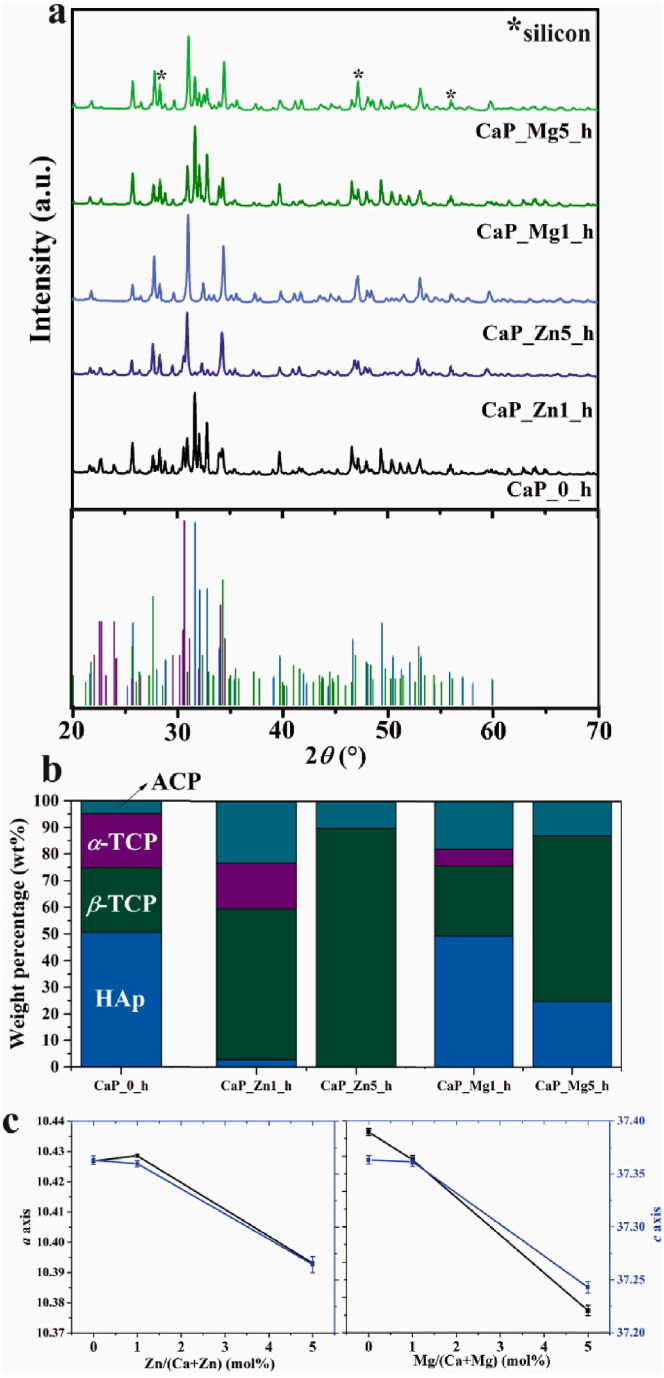

Fig. 4. (a) XRD data of the heat-treated CaP powders and (b) weight percentage of formed phases obtained by Rietveld refinement analysis. The standard ICDD card data of hydroxyapatite (blue), β-tricalcium phosphate (green) and α-tricalcium phosphate (purple) are given below XRD data. (c) Unit-cell parameters of β-tricalcium phosphate obtained by Rietveld refinement of XRD data. Silicon (standard) is marked as (*). (For interpretation of the references to color in this figure legend, the reader is referred to the Web version of this article.)

characteristic absorption bands of CO_3^{2-} in the form of out-of-plane bending (ν_2) at 868 cm^{-1}, and asymmetric stretching (ν_3) at 1408 and 1458 cm^{-1}. The absorption bands characteristic for CO_3^{2-} groups indicate B-type substitution of PO_4^{3-} by CO_3^{2-} groups [64,65]. Biological apatite is very rich in CO_3-substitution, with carbonate replacing OH^- ions in the A-site (A-type substitution) and PO_4^{3-} ions in the B-site (B-type substitution) of the apatite structure in a ratio of 1:9 [66].

3.4. SEM analysis

SEM analysis (Fig. 3b) of the as-prepared CaP powders shows agglomerated, platelet-shaped crystals. Hydroxyapatite obtained by the precipitation method can crystallize in various forms, such as sphere, rod, plate flake or flower, while OCP exhibits platelet-shaped crystals [18]. With increasing content of Zn^{2+} and Mg^{2+} ions, smaller CaP clusters are formed. Compared to Zn^{2+} ion, Mg^{2+} significantly inhibits the growth and size of CaP clusters. Smaller clusters of substituted CaP powders are in agreement with a decrease in crystallite size determined by the Rietveld refinement method. EDX analysis was used to confirm the atomic composition of the prepared substituted CaP powders. The EDX spectra (Fig. 3c) confirmed the presence of calcium, phosphorus, zinc and magnesium ions. Furthermore, EDX elemental mapping showed an uniform distribution of the elements as shown in Fig. 3d for the CaP_Zn5 and CaP_Mg5 powders. The EDS analysis did not detect Sr^{2+} and Na^{+} ions due to their low concentration determined by the ICP-MS analysis.

3.5. XRD patterns of heat-treated powders

The XRD patterns of heat-treated powders are shown in Fig. 4a. The formed crystalline phases correspond to HAp (ICDD 09-0432), β-TCP (JCPDS No. 09-0169), and α-TCP (JCPDS No. 09-0348). The sharp peaks confirm that the obtained CaP phases are highly crystallized. The quantitative phase composition (Fig. 4b) of the heat-treated CaP powders determined by Rietveld refinement of the XRD data indicates the stabilization of β-TCP phase with the increase of Zn^{2+} and Mg^{2+} substitution level. Stoichiometric HAp, free of ionic impurities, is a highly stable CaP phase up to 1400 °C. At temperatures above 1200 °C, the transformation to a β-TCP phase begins, while at 1550 °C the β-TCP phase transforms to an α-TCP phase. In addition to the stabilizing effect of Zn^{2+} and Mg^{2+} ions on the β-TCP phase, CaP_0 powder is a multi-substituted system and it is referred to as non-stoichiometric HAp with Ca/P ratio lower that 1.67, which can be transformed to TCP phases at lower temperatures than stoichiometric HAp [67]. As reported by Ren et al. [51,55], smaller substituted ions in the HAp structure lead to significant lattice strain, resulting in more defects that promote the HAp decomposition. Numerous studies have demonstrated the stabilizing effect of Zn^{2+} and Mg^{2+} on the formation of β-TCP after heat treatment [13,57,68]. The obtained results are in agreement with the findings of Bigi et al. [54,56], who reported that Zn^{2+} and Mg^{2+} ions promote the thermal conversion of HAp into β-TCP, since these ions prefer structures with available octahedral coordination sites characteristic for β-TCP. The amount of ACP in the CaP_0_h (~5 wt%) is in agreement with the study of Vecstaudza et al. [69] where ACP thermal behaviour was evaluated. After the heat treatment of the pure ACP phase at 1200 °C, the degree of the crystallinity was determined to be between 95 and 99%. In the present study, with the addition of the Mg^{2+} and Zn^{2+} ions, the amount of ACP in heat-treated samples was higher compared to sample CaP_0_h. In the study by Gross et al. [70], ACP crystallization was shifted towards higher temperatures after the incorporation of the Zn^{2+} ions in its structure. Small cations (Mg^{2+} and Zn^{2+}) have been known to stabilize the amorphous phase and prevent the crystallization process. However, even though the stabilization of the ACP phase by the introduction of small cations in the structure was reported, the effect of these ions on ACP stability at 1200 °C was not reported. Additional studies are required to understand the effect of trace elements on ACP stability at high temperatures.

Lattice parameters of HAp, β-TCP and α-TCP, determined by Rietveld refinement of XRD data, indicate preferential incorporation of Zn^{2+} and Mg^{2+} ions into the β-TCP lattice. No significant difference in cell parameters of HAp and α-TCP phase was observed (data not shown). The lattice parameters of β-TCP are shown in Fig. 4c. A gradual decrease in the $a = b$ and c axis structural parameters of β-TCP indicates the incorporation of Mg^{2+} ions at Ca(4,5) sites (Table S3 of Supplementary material), as previously observed by Enderle et al. [71]. No significant change of the lattice parameters in the β-TCP structure was observed at low Zn substitution level but decreased parameter values are evident at higher Zn substitution level. Contrary to expectations, the Zn^{2+} ion preferably occupy Ca4 site, even though it is not the spatially smallest Ca site, together with a minor occupation of Ca1, Ca2 and Ca3 sites (Supplementary material, Table S3). The trigonal crystal structure of β-TCP, with space group $R3c$, has five Ca sites, with the Ca4 site partially occupied (occ. = 0.5) [72]. The Ca–O bond lengths in the β-TCP structure are Ca1–O (0.255 nm), Ca2–O (0.247 nm), Ca3–O (0.260 nm),

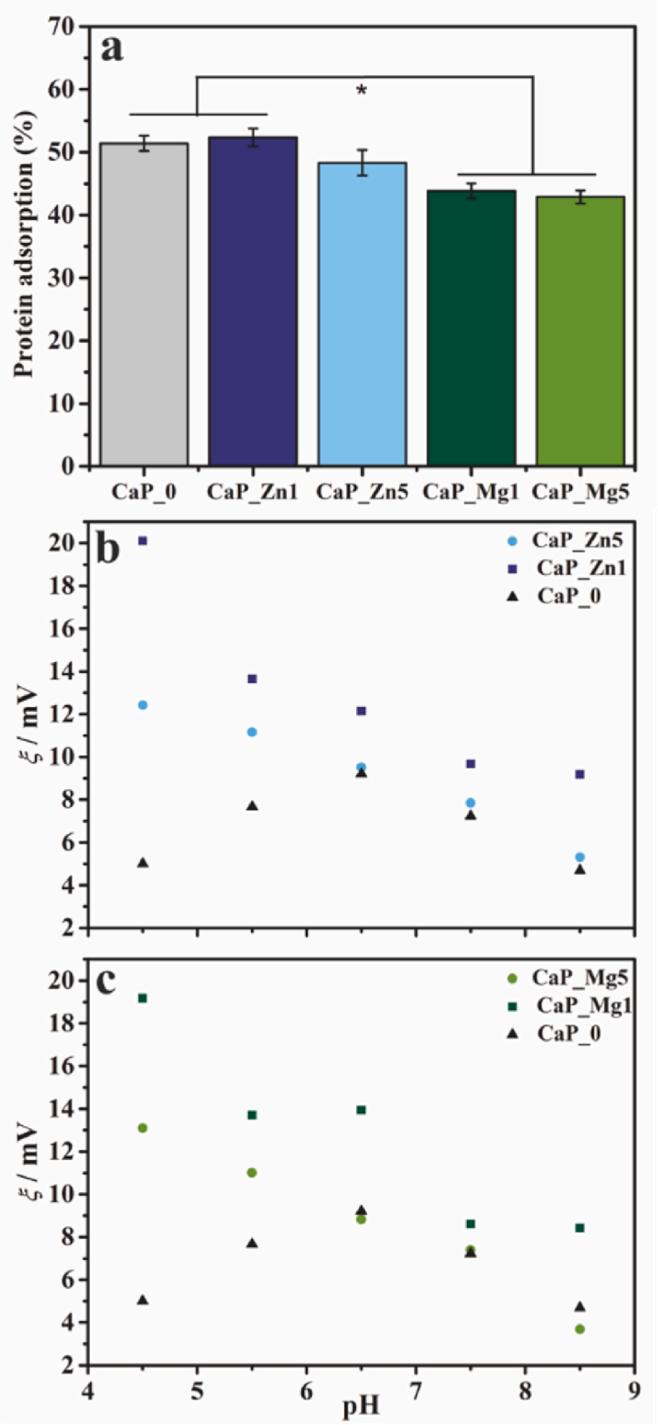

Fig. 5. (a) The protein adsorption (%) of BSA on non-substituted, Zn- and Mg-substituted CaP powders. The zeta potential of (b) Zn- and (c) Mg-substituted CaP crystals as a function of pH value.

Ca4–O (0.277 nm), and Ca5–O (0.229 nm). According to the literature, divalent cations favour substitution at sites Ca4 and Ca5, which have less disordered coordination environment. Smaller cations preferably occupy the Ca5 site due to its lower coordination number and bond length. The occupation of the Ca4 site by Zn^{2+} ions in the β-TCP structure was also observed by Gomes et al. [57]. Diverse results for the occupation of sites (Ca1,2,3) by Zn^{2+} ions may be a result of substitution of different ions in the CaP structure due to the use of a biogenic source. According to Matsunaga [72], foreign ions can influence formation energies on Ca sites, resulting in different site occupancy than in non-substituted structures.

3.6. Protein adsorption and zeta-potential measurements

Adsorption of BSA protein onto Zn- and Mg-substituted CaP powders was conducted under simulated physiological conditions at pH value of 7.4 (Fig. 5a). CaP_Zn1 showed similar protein adsorption capacity to non-substituted HAp, an insignificant decrease was observed for CaP_Zn5 sample, while significantly lower protein adsorption capacity is determined for CaP_Mg1 and CaP_Mg5 powders. However, the high BSA adsorption capacity is evident for all obtained samples (≥45%). Protein adsorption is a crucial step during bone regeneration because proteins are the basis for biomaterial interactions with cells and tissues [73]. The adsorption capacity of proteins is directly related to their charge, as well as to the surface charge of biomaterials. The pH of the solution affects the adsorption capacity of BSA, since the isoelectric point of the protein is about pH 4.5–5.0. In general, proteins are negatively charged at neutral pH and positively charged at acidic conditions [72]. Only when the isoelectric point is equal to the physiological pH, the positive and negative charges of a protein are in equilibrium and the protein is neutral in charge [74]. Böhme and Scheler [75] determined an effective charge of the BSA protein of +21.1 at low pH, while at high pH an effective charge of −17.2 was found. At the pH of the biological medium (pH = 7.4), the effective charge is about −10. Protein adsorption capacity is generally dependent on a number of surface-related properties (topography, particle size, wettability, surface charge, etc.), that affect the adhesion ability of cells [73]. To elucidate the adsorption capacity of proteins on biomaterials, in addition to protein characteristics, it is also necessary to determine the charge of the biomaterials, which is also a function of the pH and the ionic content of the solution. Characterization of the surface chemistry of CaP applying zeta-potential measurements has recently gained increasing relevance, as it directly reflects the phenomena that occur at the interface between biomaterial and surrounding tissue [76].

Characterization of zeta-potential was performed for non-substituted CaP sample (presented in both Fig. 5b and c), and for Zn-substituted (Fig. 5b) and Mg-substituted (Fig. 5c) CaP powders as a function of pH of the PBS buffer media. For the prepared CaP powders, the results showed that: (i) all samples were positively charged, (ii) positively charged samples are suitable for adsorption of negatively charged proteins due to electrostatic interactions, (iii) the obtained zeta-potential values expressed a downward trend with increasing buffer pH for substituted CaP samples, and (iv) the bell-shaped profile of the positively charged particles is evident for the non-substituted CaP system. In terms of zeta-potential values, the replacement of Ca^{2+} with isovalent ions, such as Mg^{2+} and Zn^{2+}, generally should not alter the net-surface charge. However, if the ionic radius of the foreign cation is smaller than that of Ca^{2+}, as is the case for Mg^{2+} and Zn^{2+} ions, it may be incorporated into calcium vacancies or interstitial sites between ionic groups, depending on the CaP preparation process. In both cases, the cationic substitutions affect the volume of the unit cell, as described in Section 3.1., and can therefore cause a charge imbalance that is reflected in the zeta-potential measurements. Briefly, the most-positive values of +20.11 mV (CaP_Zn1) and +19.18 mV (CaP_Mg1) were obtained in acidic PBS solution, indicating moderate colloidal stability of these substituted particles. However, considering bioceramics as implant materials, the zeta-potential values obtained under physiological conditions must be considered. The small difference in zeta-potential values obtained for Zn-substituted CaP (+9.68 mV for CaP_Zn1 and +7.84 mV for CaP_Zn5), and for Mg-substituted CaP (+8.61 mV for CaP_Mg1 and +7.40 for CaP_Mg5, respectively), is consistent with a minuscule difference in protein adsorption between the obtained powder samples (Fig. 5a). Slightly positively charged Zn-containing CaPs, obtained in simulated body fluid, were also reported by Fujii et al. [77] and Zhang et al. [78]. For Mg-substituted HAp particles, the only zeta-potential data available in the literature was the one measured in water, exhibiting negatively charged bioceramics [79]. Since BSA proteins are negatively charged when immersed in physiological fluids, they readily adsorb to positively charged surfaces due to attractive electrostatic forces [78]. Thus, since the adsorption rate is accelerated when protein and biomaterial have opposite surface charges, it can be concluded that the obtained non-substituted and substituted CaP powders have the desired properties for bone tissue engineering applications [73].

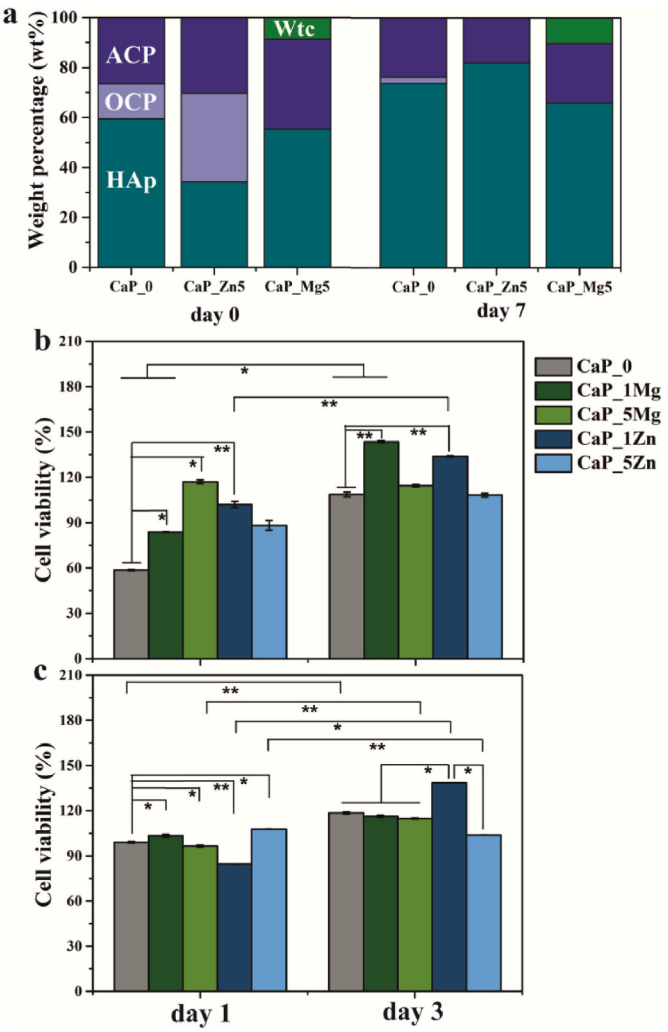

Fig. 6. (a) Results of quantitative analysis of powders after soaking in SBF, compared to as-prepared powders. (b) Biocompatibility of the extracts of the substituted CaP powders determined by MTT and (c) *Live/dead* assay. The significant difference between two groups: * ($p < 0.01$), ** ($p < 0.05$).

3.7. In vitro bioactivity and biocompatibility

The results of quantitative XRD analysis (Fig. 6a) of CaP_0, CaP_Zn5, and CaP_Mg5 powders after incubation in SBF at 37 °C for 7 days, show the partial transformation of ACP and OCP into the thermodynamically

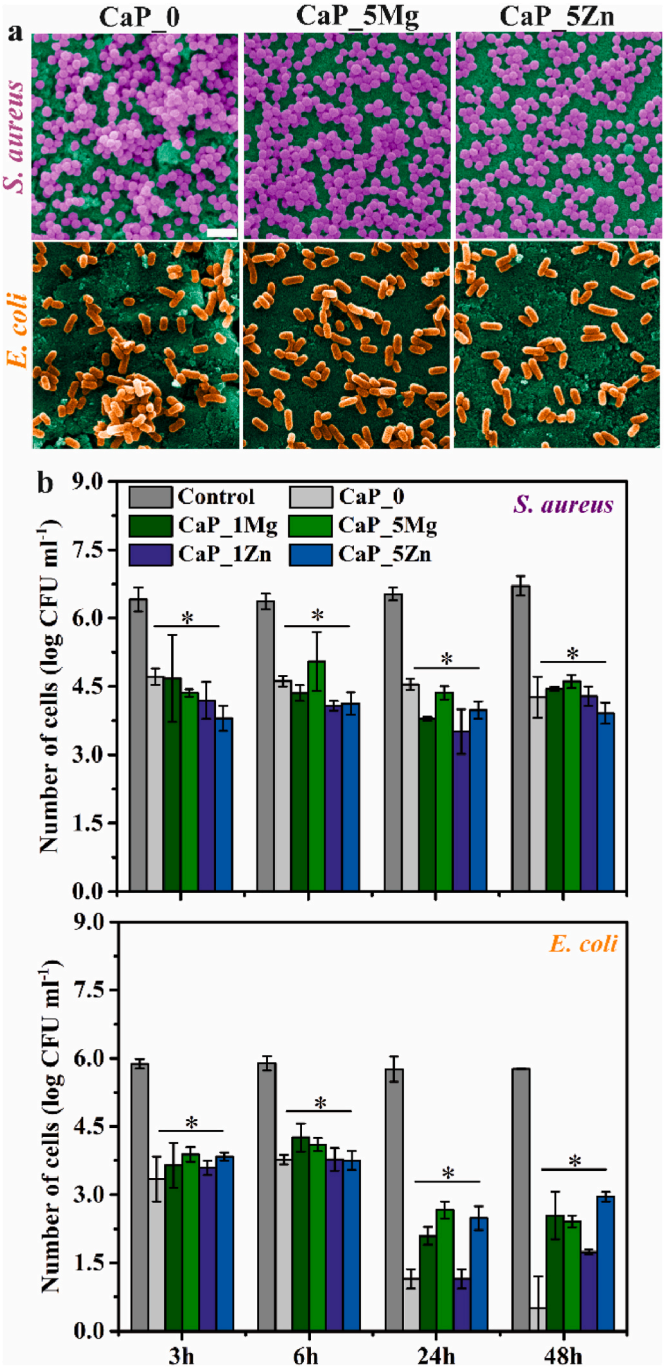

Fig. 7. (a) SEM images of *S. aureus* and *E. coli* on the discs of the prepared samples after inhibition zone analysis. The *S. aureus* were colored purple, *E. coli* orange, while the CaP surface was stained green. Scale bar: 2 μm. (b) Antibacterial efficacy of the synthesized CaP powders determined by measuring the number of viable bacterial cells in the suspension after 3, 6, 24, and 48 h. (For interpretation of the references to color in this figure legend, the reader is referred to the Web version of this article.)

more stable phase, HAp. The content of whitlockite increased slightly after the incubation of CaP_Mg5 powder. The transformation of CaPs under physiological conditions plays a crucial role in the bone regeneration process. ACP is considered a precursor phase of bone mineral in mammals and a transient phase of CaP deposition during the biomineralization of natural bones and teeth. Under physiological conditions, hydrolysis of PO_4^{3-} groups occurs, leading to the formation of HPO_4^{2-} and OH^- ions, while the resultant phase can be described as $Ca_9(PO_4)_6$-$_x(HPO_4)_x(OH)_x$. Thus, the reaction would lead to the precipitation of calcium-deficient apatite through the formation of the intermediate OCP product. ACP in prepared materials is the desired phase because such materials better mimic natural bone tissue. However, the presence of ACP in prepared materials cannot be controlled, and its weight percentage in as-prepared powders is in the range of 14–36 *wt*%, while in natural bone mineral it is in the range of 1–30 *wt*% [1,42,80]. In recent years, OCP has attracted more attention as its conversion to HAp enhances cellular activity. Implantation of OCP based materials that converted to the apatite phase results in the increase in cell proliferation and differentiation, while this effect has not been observed after incorporation of pure HAp [46,81,82].

The biocompatibility test is of great importance because high concentrations of trace elements can have a toxic effect on cells. The MTT test (Fig. 6b) and the *live/dead* assay (Fig. 6c) were performed on the obtained powder extracts. The biocompatibility is expressed through cell viability (%) and live cells (%), respectively, calculated in reference to untreated cells. The cell viability of CaP_1Mg, CaP_5Mg and CaP_1Zn powders, determined by MTT assay, is significantly higher compared to CaP_0 after 1 day of cell culture. A significant increase in cell viability is observed for CaP_0, CaP_1Mg and CaP_1Zn after 3 days of cell culture. Although the cell viability of CaP_0 samples increased significantly, the cell viability is substantially lower compared to CaP_1Mg and CaP_1Zn samples after 3 days of cell culture. The *live/dead* assay revealed a pronounced increase in the number of live cells when treated with CaP_Mg1 and CaP_Zn5 extracts, and a significant decrease in the cell number when treated with CaP_5Mg and CaP_1Zn extracts, compared to treatment with CaP_0 extracts, after 1 day of cell culture. After 3 days of cell culture, the percentage of live cells remarkably increased for CaP_0, CaP_5Mg, CaP_1Zn, while there was a significant decrease observed for CaP_5Zn. The percentage of living cells is significantly higher for the CaP_1Zn sample compared to the other obtained CaP powders after 3 days of cell culture. It may be concluded that the observed CaP systems are non-cytotoxic and promote proliferation of HEK 293, especially CaP_1Zn powder.

3.8. Antibacterial activity

SEM microscopy was applied to evaluate the surface of the CaP_0, CaP_5Mg, and CaP_5Zn powders after growth inhibition analysis toward *S. aureus* and *E. coli* (Fig. 7a). The inhibition zones were not evident for any of the evaluated CaP samples (data not shown). By examining the SEM images, the *S. aureus* and *E. coli* bacteria demonstrated no apparent difference in bacterial density population on non-substituted and Mg^{2+} or Zn^{2+} substituted CaP powders. The *S. aureus* and *E. coli* density were smaller on the CaP powders substituted with Zn^{2+} ion; however, both types of bacteria were present on the sample surface. Fig. 7b depicts the antibacterial efficacy of the prepared substituted CaP powders as determined by measuring the number of viable bacterial cells in the suspension after 3, 6, 24, and 48 h. Suspensions of *S. aureus* and *E. coli* bacteria without added CaP powders were used as controls. All prepared samples caused a reduction in the number of Gram-positive *S. aureus* bacterial cells compared to the control. However, no significant difference in bacterial viability was observed between the prepared CaP samples. The antibacterial effect is much more pronounced in the Gram-negative *E. coli* bacteria, as previously observed for the HAp substituted with Sr^{2+} and Ag^+ ions [83]. The reduction of *E. coli* cell number is not related to the change in pH, which was in the range of 8.0–8.3 after 48 h of contact with the prepared powders. Moreover, the possibility of bacterial cells attachment after 48 h of contact on CaP powders was excluded by Gram staining. The decrease in bacterial cell viability of non-substituted and Mg-substituted CaP powders may be attributed to the direct contact of the cells with the prepared CaPs nanocrystals. The same effect on *E. coli* bacterial cells was observed in our previous study for HAp substituted with Sr^{2+} and Ag^+ ions, while this effect was not observed for *S. aureus* bacterial cells [83].

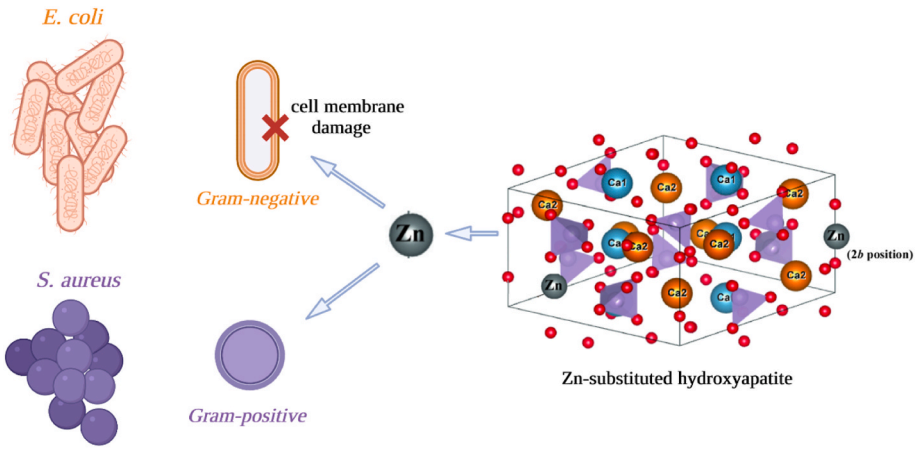

Fig. 8. Schematic illustration of antibacterial properties of substituted HAp against *E. coli* and suppressed antibacterial activity against *S. aureus*. In the HAp structure, the zinc substitution is shown on the Ca2 site and the *c*-axis in the 2b position between two oxygen ions [17]. Created with BioRender.com.

Surface charge is one factor that influences bacterial attachment and further biofilm formation. Most bacterial cells possess a net negative charge due to the high content of carboxyl, amino and phosphate groups. A negatively charged surface of biomaterials hinders bacterial attachment, while positively charged promotes adhesion of bacterial cells [84]. Zeta-potential measurements revealed a positive surface charge of all prepared CaP powders, which resulted in enhanced attachment of bacterial cell due to the attractive electrostatic forces.

The proposed mechanism of Zn–CaP antibacterial activity is related to the ability of Zn^{2+} ions to form bonds with proteins present in the cell membrane of bacteria. Binding causes a conformational change in the cell membrane proteins leading to the release of nutrients and essential components of the cytoplasm, resulting in severe damage of the cell membrane and eventual cell death. Zn^{2+} ions not only damage the cell membrane but also inhibit the activity of several enzymes [85]. In the present study, a pronounced antibacterial activity was observed against Gram-negative *E. coli* bacteria cells, whereas the same effect was not observed for Gram-positive *S. aureus,* as schematically illustrated in Fig. 8. Contrary to expectations, the antibacterial activity of the prepared Zn-substituted CaP powders was not significantly higher compared either to the Mg-substituted CaP powders or non-substituted CaP powder. The explanation of this behaviour may be in fact that the antibacterial activity of Zn^{2+} ions depends on the substitution mechanism in a crystal lattice. Bhattacharjee et al. [86] observed no antibacterial activity when Zn^{2+} ions were substituted in OH channels (2b position), which can be attributed to limited leaching of Zn^{2+} after incorporation in the 2b position, compared to the incorporation of zinc at Ca site. It can be assumed, that there is no sudden release of Zn^{2+} ions in the prepared samples and that the antibacterial effect of the Zn-substituted CaP powders could possibly be visible after a prolonged incubation period with bacterial cells. The position of the substituted ions and the occupancy of Ca sites in the CaPs lattice are rarely examined in the literature. The present study highlights the importance of knowing the position of substituted ions in biomaterials to further understand their physicochemical and biological properties. The antibacterial activity of metal ions depends on (i) the concentration of metal ions, (ii) the interactions between bacterial membrane and metal ions, and (iii) the cell membrane structure of Gram-positive and Gram-negative bacteria [85]. Gram-negative bacteria usually possess just one or few peptidoglycan sheets, as opposed to Gram-positive ones that possess very thick cell wall containing many 2D sheets of peptidoglycan, thus possibly making them more resilient to Zn^{2+} ions penetration to the inside of the cell.

This study confirmed that by using biogenic sources as precursors of Ca^{2+} ions, co-substituted CaPs, with elemental content similar to that of natural bone minerals, can be obtained [17]. Prepared multi-phase CaP powders, co-substituted with Mg^{2+}, Zn^{2+}, Sr^{2+}, Na^{+} and CO_3^{2-} ions, can be used as an inorganic component in the polymer-based scaffold as previously described in our study [87] where an increased expression of osteogenesis-related markers and increased phosphate deposits, compared to the scaffolds with non-substituted CaPs, were observed. Nowadays, studies on CaP scaffolds are focused on the fabrication of the scaffolds by additive manufacturing techniques because they allow the formation of complex designs required for bone regeneration. Obtained CaPs, substituted with Mg^{2+} and Zn^{2+} ions, can be used for scaffold development by ceramic stereolithography where printed three-dimensional scaffolds undergo a sintering process at high temperatures. Obtained results can give insights into CaP phases that can be expected after the sintering of the ceramic scaffolds.

4. Conclusion

The present study has shown that a multiphase and multi-substituted CaP system of calcium-deficient carbonated hydroxyapatite, octacalcium phosphate and amorphous calcium phosphate can be obtained from a biogenic source. The obtained materials mimic the native bone mineral in terms of phase and chemical composition. The presence of smaller sized ions in the reaction solution, (Zn^{2+} and Mg^{2+}) resulted in their incorporation into different CaP phases (hydroxyapatite, octacalcium phosphate and β-tricalcium phosphate), which affected their crystallinity, morphology and thermal stability. Octacalcium phosphate and amorphous calcium phosphate transform to a hydroxyapatite phase that is thermodynamically more stable under simulated physiological conditions. The prepared non-substituted and mono-substituted CaP powders are characterized by a positive surface potential, which favours bacterial attachment. Antibacterial effect of synthesized CaP powders against *E. coli* was observed, while the antibacterial effect against *S. aureus* was limited. All prepared powders showed high BSA protein adsorption capacity during 4 h incubation period. The obtained CaP systems are non-cytotoxic and promote proliferation of HEK 293, especially CaP_1Zn powders. Based on the presented results, it can be concluded that the prepared substituted CaP systems could be novel biomimetic ceramics for the fabrication of implants for bone tissue regeneration, as they exhibit unique biological and antibacterial properties.

Declaration of competing interest

The authors declare that they have no known competing financial interests or personal relationships that could have appeared to influence the work reported in this paper.

Acknowledgments

The financial support of European Regional Development Fund (grant KK.01.1.1.107.0014) is gratefully acknowledged. This research was conducted in part with resources from the CeSaR project (UP.03.1.1.04.0026), funded by the European Commission under the European Social Fund (ESF) 2014-2020 programme.

Appendix A. Supplementary data

Supplementary data to this article can be found online at https://doi.org/10.1016/j.ceramint.2022.11.295.

References

[1] W. Habraken, P. Habibovic, M. Epple, M. Bohner, Calcium phosphates in biomedical applications: materials for the future? Mater. Today 19 (2016) 69–87, https://doi.org/10.1016/j.mattod.2015.10.008.
[2] M. Vallet-Regi, J.M. Gonzalez-Calbet, Calcium phosphates as substitution of bone tissues, Prog. Solid State Chem. 32 (2004) 1–31, https://doi.org/10.1016/j.progsolidstchem.2004.07.001.
[3] S. Bose, G. Fielding, S. Tarafder, A. Bandyopadhyay, Trace element doping in calcium phosphate ceramics to Understand osteogenesis and angiogenesis, Trends Biotechnol. 31 (2013) 594–605, https://doi.org/10.1016/j.tibtech.2013.06.005.
[4] M.M. Stevens, Biomaterials for bone tissue engineering, Mater, Today Off. 11 (2008) 18–25, https://doi.org/10.1016/S1369-7021(08)70086-5.
[5] S.V. Dorozhkin, Biphasic, triphasic and multiphasic calcium orthophosphates, Acta Biomater. 8 (2012) 963–977, https://doi.org/10.1016/j.actbio.2011.09.003.
[6] M. Ebrahimi, M.G. Botelho, S.V. Dorozhkin, Biphasic calcium phosphates bioceramics (HA/TCP): concept, physicochemical properties and the impact of standardization of study protocols in biomaterials research, Mater. Sci. Eng. C Mater. Biol. Appl. 71 (2017) 1293–1312, https://doi.org/10.1016/j.msec.2016.11.039.
[7] E. Boanini, M. Gazzano, A. Bigi, Ionic substitutions in calcium phosphates synthesized at low temperature, Acta Biomater. 6 (2010) 1882–1894, https://doi.org/10.1016/j.actbio.2009.12.041.
[8] R.J. Friedrichs, H.F. Chappell, D.V. Shepherd, S.M. Best, Synthesis, characterization and modelling of zinc and silicate co-substituted hydroxyapatite, J. R. Soc. Interface 12 (2015), 20150190, https://doi.org/10.1098/rsif.2015.0190.
[9] K. Matsunaga, First-principles study of substitutional magnesium and zinc in hydroxyapatite and octacalcium phosphate, J. Chem. Phys. 128 (2008), 245101, https://doi.org/10.1063/1.2940337.
[10] C.L. Popa, A. Deniaud, I. Michaud-Soret, R. Guégan, M. Motelica-Heino, D. Predoi, Structural and biological assessment of zinc doped hydroxyapatite nanoparticles, 2016, J. Nanomater. (2016) 1–10, https://doi.org/10.1155/2016/1062878.
[11] W. Mróz, A. Bombalska, S. Burdyńska, M. Jedyński, A. Prokopiul, B. Budner, A. Ślósarczyk, A. Zima, E. Menaszek, A. Ścisłowska-Czarnecka, K. Niedzielski, Structural studies of magnesium doped hydroxyapatite coatings after osteoblast culture, J. Mol. Struct. 977 (2010) 145–152, https://doi.org/10.1016/j.molstruc.2010.05.025.
[12] A. Farzadi, F. Bakhshi, M. Solati-Hashjin, M. Asadi-Eydivand, N. Azuan abu Osman, Magnesium incorporated hydroxyapatite: synthesis and structural properties characterization, Ceram. Int. 40 (2014) 6021–6029, https://doi.org/10.1016/j.ceramint.2013.11.051.
[13] L. Stipniece, K. Salma-Ancane, M. Borodajenko, M. Sokolova, D. Jakovlevs, L. Berzina-Cimdina, Characterization of Mg-substituted hydroxyapatite synthesized by wet chemical method, Ceram. Int. 40 (2014) 3261–3267, https://doi.org/10.1016/j.ceramint.2013.09.110.
[14] A. Bhattacharjee, A. Gupa, M. Verma, P.A. Murugan, P. Sengupta, S. Matheshwaran, I. Manna, K. Balani, Site-specific antibacterial efficacy and cyto/hemo-compatibility of zinc substituted hydroxyapatite, Ceram. Int. 45 (2019) 12225–12233, https://doi.org/10.1016/j.ceramint.2019.03.132.
[15] A. Anwar, S. Akbar, A. Sadiqa, M. Kazmi, Novel continuous flow synthesis, characterization and antibacterial studies of nanoscale zinc substituted hydroxyapatite bioceramics, Inorg. Chim. Acta. 453 (2016) 16–22, https://doi.org/10.1016/j.ica.2016.07.041.
[16] Y. Ben, C. Fu, M. Hu, L. Liu, M. Huang Wong, C. Zheng, Human health risk assessment of antibiotic resistance associated with antibiotic residues in the environment: a review, Environ. Res. 169 (2019) 483–493, https://doi.org/10.1016/j.envres.2018.11.040.
[17] A. Ressler, A. Žužić, I. Ivanišević, N. Kamboj, H. Ivanković, Ionic substituted hydroxyapatite for bone regeneration applications: a review, Open Ceramics 6 (2021), 100122, https://doi.org/10.1016/j.oceram.2021.100122.
[18] M. Sadat-Shojai, M.T. Khorasani, E. Dinpanah-Khoshdargi, A. Jamshidi, Synthesis methods for nanosized hydroxyapatite with diverse structures, Acta Biomater. 9 (2013) 7591–7621, https://doi.org/10.1016/j.actbio.2013.04.012.
[19] S. Scialla, F. Carella, M. Dapporto, S. Sprio, A. Piancastelli, B. Palazzo, A. Adamiano, L. Degli Esposti, M. Iafisco, C. Piccirillo, Mussel shell-derived macroporous 3D scaffold: characterization and optimization study of a bioceramic from the circular economy, Mar. Drugs 18 (2020) 309, https://doi.org/10.3390/md18060309.
[20] G. Falini, M.L. Basile, S. Gandolfi, F. Carella, G. Guarini, L. Degli Esposti, M. Iafisco, A. Adamiano, Natural calcium phosphates from circular economy as adsorbent phases for the remediation of textile industry waste-waters, Ceram. Int. (2022), https://doi.org/10.1016/j.ceramint.2022.08.337. In Press.
[21] A. Ressler, M. Cvetnić, M. Antunović, I. Marijanović, M. Ivanković, H. Ivanković, Strontium substituted biomimetic calcium phosphate system derived from cuttlefish bone, J. Biomed. Mater. Res. B Appl. Biomater. 18 (2019) 1697–1709, https://doi.org/10.1002/jbm.b.34515.
[22] A. Ressler, M. Antunović, M. Cvetnić, M. Ivanković, H. Ivanković, Selenite substituted calcium phosphates: preparation, characterization, and cytotoxic activity, Materials 14 (2021) 3436, https://doi.org/10.3390/ma14123436.
[23] G. Suresh Kumar, E.K. Girija, Flower-like hydroxyapatite nanostructure obtained from eggshell: a candidate for biomedical applications, Ceram. Int. 39 (2013) 8293–8299, https://doi.org/10.1016/j.ceramint.2013.03.099.
[24] C.M. Mardziah, S. Ramesh, C.Y. Tan, H. Chandran, A. Sidhu, S. Krishnasamy, J. Purbolaksono, Zinc-substituted hydroxyapatite produced from calcium precursor derived from eggshells, Ceram. Int. 47 (2021) 33010–33019, https://doi.org/10.1016/j.ceramint.2021.08.201.
[25] S. Lala, M. Ghosh, P.K. Das, D. Das, T. Kar, S.K. Pradhan, Magnesium substitution in carbonated hydroxyapatite: structural and microstructural characterization by Rietveld's refinement, Mater. Chem. Phys. 170 (2016) 319–329, https://doi.org/10.1016/j.matchemphys.2015.12.058.
[26] F. Miyaji, Y. Kono, Y. Suyama, Formation and structure of zinc-substituted calcium hydroxyapatite, Mater. Res. Bull. 40 (2005) 209–220, https://doi.org/10.1016/j.materresbull.2004.10.020.
[27] Lj. Veselinović, Lj. Karanović, Z. Stojanović, I. Bračko, S. Marković, N. Ignjatović, D. Uskoković, Crystal structure of cobalt-substituted calcium hydroxyapatite nanopowders prepared by hydrothermal processing, J. Appl. Crystallogr. 43 (2010) 320–327, https://doi.org/10.1107/S0021889809051395/ks5226sup2.rtv.
[28] M. Espanol, J. Portillo, J.M. Manero, M.P. Ginebra, Investigation of the hydroxyapatite obtained as hydrolysis product of atricalcium phosphate by transmission electron microscopy, CrystEngComm 12 (2010) 3318–3326, https://doi.org/10.1039/C001754J.
[29] M. Yashima, A. Sakai, T. Kamiyama, A. Hoshikawa, Crystal structure analysis of β-tricalcium phosphate Ca3(PO4)2 by neutron powder diffraction, J. Solid State Chem. 175 (2003) 272–277, https://doi.org/10.1016/S0022-4596(03)00279-2.
[30] M. Mathew, W.E. Brown, L.W. Schroeder, B. Dickens, The crystal structure of alpha-$Ca_3(PO_4)_2$, Acta Crystallogr. B 33 (1977) 1325–1333, https://doi.org/10.1107/S0567740877006037.
[31] C. Shi, J. Gao, M. Wang, J. Fu, D. Wang, Y. Zhu, Ultra-trace silver-doped hydroxyapatite with non-cytotoxicity and effective antibacterial activity, Mater. Sci. Eng. C 55 (2015) 497–505, https://doi.org/10.1016/j.msec.2015.05.078.
[32] M. Bohner, J. Lemaitre, Can bioactivity be tested in vitro with SBF solution? Biomaterials 30 (2009) 2175–2179, https://doi.org/10.1016/j.biomaterials.2009.01.008.
[33] B. Ben-Nissan, Natural bioceramics: from coral to bone and beyond, Curr. Opin. Solid State Mater. Sci. 7 (2003) 283–288, https://doi.org/10.1016/j.cossms.2003.10.001.
[34] B.S. Kim, H.J. Kang, S.S. Yang, J. Lee, Comparison of in vitro and in vivo bioactivity: cuttlefish-bone-derived hydroxyapatite and synthetic hydroxyapatite granules as a bone graft substitute, Biomed. Mater. 9 (2014), 025004, https://doi.org/10.1088/1748-6041/9/2/025004.
[35] K. Matsunaga, H. Murata, Formation energies of substitutional sodium and potassium in hydroxyapatite, Mater. Trans. 50 (2009) 1041–1045, https://doi.org/10.2320/matertrans.MC200819.
[36] M.E. Fleet, X. Liu, Coupled substitution of type A and B carbonate in sodium-bearing apatite, Biomaterials 28 (2007) 916–926, https://doi.org/10.1016/j.biomaterials.2006.11.003.
[37] E. Landi, G. Celotti, G. Logroscino, A. Tampieri, Carbonated hydroxyapatite as bone substitute, J. Eur. Ceram. Soc. 23 (2003) 2931–2937, https://doi.org/10.1016/S0955-2219(03)00304-2.
[38] M.E. Fleet, X. Liu, X. Liu, Orientation of channel carbonate ions in apatite: effect of pressure and composition, Am. Min. 96 (2011) 1148–1157, https://doi.org/10.2138/am.2011.3683.
[39] J.D. Birchall, N.L. Thomas, On the architecture and function of cuttlefish bone, J. Mater. Sci. 18 (1983) 2081–2086, https://doi.org/10.1007/BF00555001.
[40] R.A. Hewitt, Analysis of aragonite from the cuttlefish bone of Sephia Officinalis L, Mar. Geol. 18 (1975), https://doi.org/10.1016/0025-3227(75)90033-X. M1-M5.
[41] J. Jeong, J.H. Kim, J.H. Shim, N.S. Hwang, C.Y. Heo, Bioactive calcium phosphate materials and applications in bone regeneration, Biomater. Res. 23 (2019) 4, https://doi.org/10.1186/s40824-018-0149-3.
[42] S.V. Dorozhkin, Amorphous calcium (ortho)phosphates, Acta Biomater. 6 (2010) 4457–4475, https://doi.org/10.1016/j.actbio.2010.06.031.
[43] Y. Sugiura, Y. Makita, Sodium induces octacalcium phosphate formation and enhances its layer structure by affecting to hydrous layer phosphate, Cryst. Growth Des. 18 (2018) 6165–6171, https://doi.org/10.1021/acs.cgd.8b01030.
[44] A. Ressler, I. Ivanišević, A. Žužić, N. Somers, The ionic substituted octacalcium phosphate for biomedical applications: a new pathway to follow? Ceram. Int. 48 (2022) 8838–8851, https://doi.org/10.1016/j.ceramint.2021.12.126.
[45] S. Von Euw, Y. Wang, G. Laurent, C. Drouet, F. Babonneau, N. Nassif, T. Azais, Bone mineral: new insights into its chemical composition, Scientific Reports 9 (2019) 1–11, https://doi.org/10.1038/s41598-019-44620-6, 8456.
[46] O. Suzuki, S. Kamakura, T. Katagiri, M. Nakamura, B. Zhao, Y. Honda, R. Kamijo, Bone formation enhanced by implanted octacalcium phosphate involving conversion into Ca-deficient hydroxyapatite, Biomaterials 27 (2006) 2671–2681, https://doi.org/10.1016/j.biomaterials.2005.12.004.

[47] K. Kobayashi, T. Anada, T. Handa, N. Kanda, M. Yoshinari, T. Takahashi, O. Suzuki, Osteoconductive property of a mechanical mixture of octacalcium phosphate and amorphous calcium phosphate, ASC Appl. Mater. Interfaces 6 (2014) 22602–22611, https://doi.org/10.1021/am5067139.
[48] F. Miyaji, Y. Kono, Y. Suyama, Formation and structure of zinc-substituted calcium hydroxyapatite, Mater. Res. Bull. 40 (2005) 209–220, https://doi.org/10.1016/j.materresbull.2004.10.020.
[49] V. Stanić, S. Dimitrijević, J. Antić-Stanković, M. Mitrić, B. Jokić, I.B. Plaćaš, S. Raičević, Synthesis, characterization and antimicrobial activity of copper and zinc-doped hydroxyapatite nanopowders, Appl. Surf. Sci. 256 (2010) 6083–6089, https://doi.org/10.1016/j.apsusc.2010.03.124.
[50] V. Aina, G. Lusvardi, B. Annaz, I.R. Gibson, F.E. Imrie, G. Malavasi, L. Menabue, G. Cerrato, G. Martra, Magnesium- and strontium-co-substituted hydroxyapatite: the effects of doped-ions on the structure and chemico-physical properties, J. Mater. Sci. Mater. Med. 23 (2012) 2867–2879, https://doi.org/10.1007/s10856-012-4767-3.
[51] F. Ren, Y. Leng, X. Ge, Synthesis, characterization and ab initio simulation of magnesium-substituted hydroxyapatite, Acta Biomater. 6 (2010) 2787–2796, https://doi.org/10.1016/j.actbio.2009.12.044.
[52] W.L. Suchanek, K. Byrappa, P. Shuk, R.E. Riman, V.F. Janas, K.S. TenHuisen, Preparation of magnesium-substituted hydroxyapatite powders by the mechanochemical–hydrothermal method, Biomaterials 25 (2004) 4647–4657, https://doi.org/10.1016/j.biomaterials.2003.12.008.
[53] M. Šupova, Substituted hydroxyapatites for biomedical applications: a review, Ceram. Int. 41 (2015) 9203–9231, https://doi.org/10.1016/j.ceramint.2015.03.316.
[54] A. Bigi, G. Falini, E. Foresti, M. Gazzano, A. Ripamonti, N. Roveri, Rietveld structure refinements of calcium hydroxylapatite containing magnesium, Acta Crystallogr. B52 (1996) 87–92, https://doi.org/10.1107/S0108768195008615.
[55] F. Ren, R. Xin, X. Ge, Y. Leng, Characterization and structural analysis of zinc-substituted hydroxyapatites, Acta Biomater. 5 (2009) 3141–3149, https://doi.org/10.1016/j.actbio.2009.04.014.
[56] A. Bigi, E. Foresti, M. Gandolfi, M. Gazzano, N. Roveri, Inhibiting effect of zinc on hydroxyapatite crystallization, J. Inorg. Biochem. 58 (1995) 49–58, https://doi.org/10.1021/jp9939726.
[57] S. Gomes, J.M. Nedelec, G. Renaudin, On the effect of temperature on the insertion of zinc into hydroxyapatite, Acta Biomater. 8 (2012) 1180–1189, https://doi.org/10.1016/j.actbio.2011.12.003.
[58] N.D. Ravi, R. Balu, T.S.S. Kumar, Strontium-substituted calcium deficient hydroxyapatite nanoparticles: synthesis, characterization, and antibacterial properties, J. Am. Ceram. Soc. 95 (2012) 2700–2708, https://doi.org/10.1111/j.1551-2916.2012.05262.x.
[59] A. Rogina, P. Rico, G. Gallego Ferrer, M. Ivanković, H. Ivanković, Effect of in situ formed hydroxyapatite on microstructure offreeze-gelled chitosan-based biocomposite scaffolds, Eur. Polym. J. 68 (2015) 278–287, https://doi.org/10.1016/j.eurpolymj.2015.05.004.
[60] J. Gao, M. Wang, C. Shi, L. Wang, Y. Zhu, D. Wang, A facile green synthesis of trace Si, Sr and F multi-doped hydroxyapatite with enhanced biocompatibility and osteoconduction, Mater. Lett. 196 (2017) 406–409, https://doi.org/10.1016/j.matlet.2017.03.054.
[61] H. Shi, F. He, J. Ye, Synthesis and structure of iron- and strontium-substituted octacalcium phosphate: effects of ionic charge and radius, J. Mater. Chem. B 4 (2016) 1712–1719, https://doi.org/10.1039/C5TB02247A.
[62] J. Terra, E.R. Dourado, J.G. Eon, D.E. Ellis, The structure of strontium-doped hydroxyapatite: an experimental and theoretical study, Phys.l Chem. Chem. Phys. 11 (2009) 568–577, https://doi.org/10.1039/B802841A.
[63] M.P. Moreira, G.D. de Almeida Soares, J. Dentzer, K. Anselme, L.A. de Sena, A. Kuznetsov, E.A. dos Santos, Synthesis of magnesium- and manganese-doped hydroxyapatite structures assisted by the simultaneous incorporation of strontium, Mater. Sci. Eng. C 62 (2016) 736–743, https://doi.org/10.1016/j.msec.2016.01.004.
[64] I.R. Gibson, W. Bonfield, Novel synthesis and characterization of an AB-type carbonate-substituted hydroxyapatite, J. Biomed. Mater. Res. 59 (2002) 697–708, https://doi.org/10.1002/jbm.10044.
[65] J.P. Lafon, E. Champion, D. Bernache-Assollant, Processing of AB-type carbonated hydroxyapatite Ca10−x(PO4)6−x(CO3)x(OH)2−x−2y(CO3)y ceramics with controlled composition, J. Eur. Ceram. Soc. 28 (2008) 139–147, https://doi.org/10.1016/j.jeurceramsoc.2007.06.009.
[66] A. Bigi, E. Boanini, M. Gazzano, Ion substitution in biological and synthetic apatites, in: C. Aparicio, M. Pau Ginebra (Eds.), Biomineralization and Biomaterials, Fundamentals and Application, Woodhead Publishing, 2016, pp. 235–266.
[67] A. Krajewski, A. Rawaglioli, Biocermaics and biological glasses, in: R. Barbucci (Ed.), Integrated Biomaterials Science, Springer, Boston, 2002, pp. 189–254.
[68] P. Bhattacharjee, H. Begam, A. Chanda, S.K. Nandi, Animal trial on zinc doped hydroxyapatite: a case study, J. Asian Ceram. Soc. 2 (2014) 44–51, https://doi.org/10.1016/j.jascer.2014.01.005.
[69] J. Vecstaudza, M. Gasik, J. Locs, Amorphous calcium phosphate materials: formation, structure and thermal behaviour, J. Eur. Ceram. Soc. 39 (2019) 1642–1649, https://doi.org/10.1016/j.jeurceramsoc.2018.11.003.
[70] K. Gross, L. Komarovska, A. Viksna, Efficient zinc incorporation in hydroxyapatite through crystallization of an amorphous phase could extend the properties of zinc apatites, J. Aust. Ceram. 49 (2013) 129–135.
[71] R. Enderle, F. Götz-Neunjoeffer, M. Göbbels, F.A. Müller, P. Greil, Influence of magnesium doping on the phase transformation temperature of b-TCP ceramics examined by Rietveld refinement, Biomaterials 26 (2005) 3379–3384, https://doi.org/10.1016/j.biomaterials.2004.09.017.
[72] K. Matsunaga, T. Kubota, K. Toyoura, A. Nakamura, First-principles calculations of divalent substitution of Ca^{2+} in tricalcium phosphates, Acta Biomater. 23 (2015) 329–337, https://doi.org/10.1016/j.actbio.2015.05.014.
[73] H.P. Felgueiras, J.C. Antunes, M.C.L. Martins, M.A. Barbosa, 1 - fundamentals of protein and cell interactions in biomaterials, in: s), Mário A. Barbosa, M. Cristina L. Martins (Eds.), Peptides and Proteins as Biomaterials for Tissue Regeneration and Repair, Woodhead Publishing, 2018, pp. 1–27, https://doi.org/10.1016/B978-0-08-100803-4.00001-2.
[74] H.T.M. Phan, S. Bartelt-Hunt, K.B. Rodenhausen, M. Schubert, J.C. Bartz, Investigation of bovine serum albumin (BSA) attachment onto self-assembled monolayers (SAMs) using combinatorial quartz crystal microbalance with dissipation (QCM-D) and spectroscopic ellipsometry (SE), PLoS One 10 (2015), e0141282, https://doi.org/10.1371/journal.pone.0141282.
[75] U. Böhme, U. Scheler, Effective charge of bovine serum albumin determined by electrophoresis NMR, Chem. Phys. Lett. 435 (2007) 342–345, https://doi.org/10.1016/j.cplett.2006.12.068.
[76] V. Uskoković, R. Odsinada, S. Djordjevic, S. Habelitz, Dynamic light scattering and zeta potential of colloidal mixtures of amelogenin and HAp in calcium and phosphate rich ionic milieus, Arch. Oral Biol. 56 (2011) 521–532, https://doi.org/10.1016/j.archoralbio.2010.11.011.
[77] E. Fujii, M. Ohkubo, K. Tsuru, S. Hayakawa, A. Osaka, K. Kawabata, C. Bonhomme, F. Babonneau, Selective protein adsorption property and characterization of nano-crystalline zinc-containing hydroxyapatite, Acta Biomater. 2 (2006) 69–74, https://doi.org/10.1016/j.actbio.2005.09.002.
[78] W. Zhang, X. Xu, Y. Chai, Y. Wang, Synthesis and characterization of Zn^{2+} and SeO_3^{2-} co-substituted nano-hydroxyapatite, Adv. Powder Technol. 27 (2016) 1857–1861, https://doi.org/10.1016/j.apt.2016.03.026.
[79] D. Predoi, S.L. Iconaru, M.V. Predoi, G.E. Stan, N. Buton, Synthesis, characterization, and antimicrobial activity of magnesium-doped HAp suspensions, Nanomaterials 9 (2019) 1295, 0.3390/nano9091295.
[80] C. Combes, C. Rey, Amorphous calcium phosphates: synthesis, properties and uses in biomaterials, Acta Biomater. 6 (2010) 3362–3378, https://doi.org/10.1016/j.actbio.2010.02.017.
[81] S. Kamakura, Y. Sasano, T. Shimizu, K. Hatori, O. Suzuki, M. Kagayama, K. Motegi, Implanted octacalcium phosphate is more resorbable than beta-tricalcium phosphate and hydroxyapatite, J. Biomed. Mater. Res. 59 (2002) 29–34, https://doi.org/10.1002/jbm.1213.
[82] N. Ito, M. Kamitakahara, K. Ioku, Observation of transformation behavior of octacalcium phosphate to hydroxyapatite, Key Eng. Mater. 529−530 (2013) 11–14. https://doi.org/10.4028/www.scientific.net/KEM.529-530.11.
[83] A. Ressler, T. Ivanković, B. Polak, I. Ivanišević, M. Kovačić, I. Urlić, I. Hussainova, H. Ivanković, A multifunctional strontium/silver-co-substituted hydroxyapatite derived from biogenic source as antibacterial biomaterial, Ceram. Int. 48 (2022) 18361–18373, https://doi.org/10.1016/j.ceramint.2022.03.095.
[84] K. Mediaswanti, Influence of physicochemical aspects of substratum nanosurface on bacterial attachment for bone implant applications, 2016, J. Nanotechnol. (2016), 5026184, https://doi.org/10.1155/2016/5026184.
[85] A. Anwar, S. Akbar, A. Sadiqa, M. Kazmi, Novel continuous flow synthesis, characterization and antibacterial studies of nanoscale zinc substituted hydroxyapatite bioceramics, Inorg. Chim. Acta. 453 (2016) 16–22, https://doi.org/10.1016/j.ica.2016.07.041.
[86] A. Bhattacharjee, A. Gupta, M. Verma, P.A. Murugan, P. Sengupta, S. Matheshwaran, I. Manna, K. Balani, Site-specific antibacterial efficacy and cyto/hemo-compatibility of zinc substituted hydroxyapatite, Ceram. Int. 45 (2019) 12225–12233, https://doi.org/10.1016/j.ceramint.2019.03.132.
[87] A. Ressler, M. Antunović, L. Teruel-Biosca, G. Gallego Ferrer, S. Babić, I. Urlić, M. Ivanković, H. Ivanković, Osteogenic differentiation of human mesenchymal stem cells on substituted calcium phosphate/chitosan composite scaffold, Carbohydr. Polym. 277 (2022), 118883, https://doi.org/10.1016/j.carbpol.2021.118883.